Tirasemtiv enhances submaximal muscle tension in an Acta1 :p.Asp286Gly mouse model of nemaline myopathy

Ricardo A Galli, Tamara C Borsboom, Charlotte Gineste, Lorenza Brocca, Maira Rossi, Darren T Hwee, Fady I Malik, Roberto Bottinelli, Julien Gondin, Maria-Antonietta Pellegrino, et al.

JGP Journal of General Physiology

ARTICLE

Tirasemtiv enhances submaximal muscle tension in an *Acta1*:p.Asp286Gly mouse model of nemaline myopathy

Ricardo A. Galli[1,2], Tamara C. Borsboom[1], Charlotte Gineste[5], Lorenza Brocca[6], Maira Rossi[6], Darren T. Hwee[7], Fady I. Malik[7], Roberto Bottinelli[6,9], Julien Gondin[5,10], Maria-Antonietta Pellegrino[6], Josine M. de Winter[1,2,3], and Coen A.C. Ottenheijm[1,4,8]

Nemaline myopathies are the most common form of congenital myopathies. Variants in *ACTA1* (NEM3) comprise 15–25% of all nemaline myopathy cases. Patients harboring variants in *ACTA1* present with a heterogeneous disease course characterized by stable or progressive muscle weakness and, in severe cases, respiratory failure and death. To date, no specific treatments are available. Since NEM3 is an actin-based thin filament disease, we tested the ability of *tirasemtiv*, a fast skeletal muscle troponin activator, to improve skeletal muscle function in a mouse model of NEM3, harboring the patient-based p.Asp286Gly variant in *Acta1*. Acute and long-term *tirasemtiv* treatment significantly increased muscle contractile capacity at submaximal stimulation frequencies in both fast-twitch extensor digitorum longus and gastrocnemius muscle, and intermediate-twitch diaphragm muscle in vitro and in vivo. Additionally, long-term *tirasemtiv* treatment in NEM3 mice resulted in a decreased respiratory rate with preserved minute volume, suggesting more efficient respiration. Altogether, our data support the therapeutic potential of fast skeletal muscle troponin activators in alleviating skeletal muscle weakness in a mouse model of NEM3 caused by the *Acta1*:p.Asp286Gly variant.

Introduction

Nemaline myopathies (NEM) are among the most common forms of congenital myopathies (Colombo et al., 2015) and compose a group of genetically heterogeneous disorders characterized by skeletal muscle weakness (Wallgren-Pettersson et al., 2011). NEM disease severity ranges from neonatally severe to a mildly progressive phenotype (Sanoudou and Beggs, 2001; Ryan et al., 2001). Histopathologically, NEM patient's muscle biopsies are characterized by the accumulation of nemaline bodies, a fiber type shift toward type 1 fibers, and in severe cases, disarrangement of the myofibrillar architecture (Yin et al., 2014). To date, 13 genes have been implicated in NEM. α-Skeletal-actin 1 (*ACTA1*) (Ilkovski et al., 2001); α- and β-tropomyosin (*TPM3* and *TPM2*) (Donner et al., 2002; Laing et al., 1995); nebulin (*NEB*) (Pelin et al., 1999); leiomodin-3 (*LMOD3*) (Yuen et al., 2015); troponin T, slow skeletal type (*TNNT1*) (Johnston et al., 2000), and Troponin T3, fast skeletal type (*TNNT3*) (Sandaradura et al., 2018); cofilin 2 (*CFL2*) (Agrawal et al., 2007); unconventional myosin 18B (*MYO18B*) (Malfatti et al., 2015); myopalladin (*MYPN*) (Miyatake et al., 2017); Kelch family members 40 (*KLHL40*) and 41 (*KLHL41*) (Gupta et al., 2013; Ravenscroft et al., 2013); and Kelch repeat and BTB (POZ) domain containing 13 (*KBTBD13*) (Sambuughin et al., 2010). 12 of these genes code for proteins that are associated with the thin filament, a key component of the skeletal muscle sarcomere. Variants in these genes result in sarcomeric dysfunction (Ochala, 2008; de Winter and Ottenheijm, 2017; Ottenheijm et al., 2010; Ochala et al., 2010, Winter et al., 2016, de Winter et al., 2020). No specific treatments are currently available.

Nemaline myopathy type 3 (NEM3) is caused by variants in the skeletal muscle α-actin gene (*ACTA1*) and comprises the second most common form of NEM (15–25% of all cases [Wallgren-Pettersson et al., 2011]). In vitro studies showed that variants in *ACTA1* affect thin filament structure and function

[1]Amsterdam UMC Location Vrije Universiteit Amsterdam, Physiology, Amsterdam, The Netherlands; [2]Amsterdam Movement Sciences, Musculoskeletal Health and Tissue Function and Regeneration, Amsterdam, The Netherlands; [3]Amsterdam Cardiovascular Sciences, Heart Failure and Arrhythmias, Amsterdam, The Netherlands; [4]Amsterdam Cardiovascular Sciences, Pulmonary Hypertension and Atherosclerosis, Amsterdam, The Netherlands; [5]Aix-Marseille University, CNRS, CRMBM, Marseille, France; [6]Department of Molecular Medicine, University of Pavia, Pavia, Italy; [7]Research and Early Development, Cytokinetics Inc., South San Francisco, CA, USA; [8]Department of Cellular and Molecular Medicine, University of Arizona, Tucson, AZ, USA; [9]IRCCS Mondino Foundation, Pavia, Italy; [10]Institut NeuroMyoGène, Unité Physiopathologie et Génétique du Neurone et du Muscle, Université Claude Bernard Lyon 1, CNRS UMR 5261, INSERM U1315, Université Lyon, Lyon, France.

Correspondence to Coen A.C. Ottenheijm: c.ottenheijm@amsterdamumc.nl.

(Vandamme et al., 2009; Marston et al., 2004), and the variants contribute to contractile weakness as assessed in vitro and in vivo (Gineste et al., 2013b; Ochala et al., 2015; Ochala et al., 2012; Lindqvist et al., 2013; Ravenscroft et al., 2011a; Joureau et al., 2018; Nguyen et al., 2011). Thus, restoring thin filament function may prove as a useful therapy to ameliorate muscle weakness in NEM3 patients.

Tirasemtiv (CK-2017357) is a fast skeletal muscle troponin activator, which increases the binding of calcium to the troponin complex (Li et al., 2021) and augments the force-generating capacity at submaximal nerve stimulations in rodents and humans (Russell et al., 2012; Hansen et al., 2014; Andrews et al., 2018). In vitro treatment with *tirasemtiv* has been shown to increase muscle strength in NEM2 (caused by variants in *NEB*) and in other neuromuscular disorders (Lee et al., 2019; Hwee et al., 2014; van de Locht et al., 2021; de Winter et al., 2013). Recently, we investigated the acute and long-term effect of *tirasemtiv* in a mouse model for severe NEM3 due to the heterozygous NM_009606.3 (Acta1):p.His40Tyr variant in *Acta1* (referred to as *Acta1*(H40Y)). *Tirasemtiv* had a positive acute and long-term effect on muscle force with a reduction in the energetic cost of contraction (de Winter et al., 2021).

It is unknown whether *tirasemtiv* has a similar positive inotropic effect on muscles in milder forms of NEM3, which have a smaller therapeutic window. Therefore, in this study, we tested the in vitro and in vivo effect of *tirasemtiv* on skeletal muscle function in a mouse model that recapitulates a mild form of NEM3 caused by the patient-based (Acta1):p.Asp286Gly variant in *Acta1* (Joureau et al., 2018). We hypothesized that both acute and long-term *tirasemtiv* treatment would increase skeletal muscle force at submaximal stimulation frequencies. Furthermore, we studied protein oxidation and pathways controlling proteostasis, e.g., ubiquitin-proteosome pathway, and mitochondrial dynamics to assess whether they were altered in this variant of NEM3 and could be involved in *tirasemtiv* impact on skeletal muscle contractility.

Throughout the manuscript, variant (Acta1):p.Asp286Gly is referred to as *Acta1*(D286G) to be consistent with existing literature (Ravenscroft et al., 2011a). Our results show that *Acta1*(D286G) mice had significantly lower hind limb muscle mass as compared to wild type mice. Acute and long-term *tirasemtiv* treatment significantly increased in vitro force production at submaximal stimulation frequencies in extensor digitorum longus (EDL) and diaphragm and reduced fatigability in the EDL muscle. Long-term *tirasemtiv* treatment showed improved in vivo contractility of gastrocnemius (GAS) muscle at submaximal stimulation frequencies. Myofibrillar proteins and myosin oxidation changes could not explain the impact of *tirasemtiv* on contractility. Together, these findings highlight the therapeutic potential of fast skeletal troponin activators to alleviate skeletal muscle weakness in mild forms of NEM3.

Materials and methods

Acta1(D286G) mouse model

Transgenic 8–12 mo-old male mice expressing the ACTA1 protein harboring the D286G variant p.Asp286Gly mutation in *Acta1* (referred to as *Acta1*(D286G)) and wild type littermates were used for the experiments (Ravenscroft et al., 2011b). Experiments were conducted in agreement with the French and Dutch guidelines for animal care. All animal experiments were approved by the Institutional Animal Care Committee of Aix-Marseille University (#15–14052012) and by the local animal ethics committee at VU University (AVD114002016501). Mice were housed in an environment-controlled facility (12–12 h light-dark cycle, 22°C), and received water and standard food ad libitum. Mice were identified through PCR genotyping from mouse tail DNA. All mice survived the study and had a normal life span.

Tirasemtiv treatment

For the experiments in which the acute effect of *tirasemtiv* was studied, mice were I.P. injected with vehicle or 3 mg/kg *tirasemtiv* (Hwee et al., 2014). Experiments were performed ∼30 min after injection. For the experiments in which muscle contractility was studied in vitro, 3 µM *tirasemtiv* was added to the experimental solutions. For the studies in which the long-term effects of *tirasemtiv* were studied, 8-mo-old mice were first fed for 1 wk with custom-made mouse pellets (BioServ). After 1 wk, mice were switched to the same pellets containing *tirasemtiv* (600 ppm) or the same pellets without *tirasemtiv*. Mice were kept on the chow for 4 wk. Whole-muscle contractility and respiratory function were tested before treatment and after 4 wk of *tirasemtiv*-enriched diet or regular diet. After 4 wk, mice were euthanized and tissues were collected, i.e., tibialis anterior (TA), EDL, soleus (SOL), GAS, and diaphragm. Blood was collected to determine plasma concentrations of *tirasemtiv*, but we did not measure its concentration in skeletal muscles. Therefore, we do not know *tirasemtiv* exposure levels in muscles during the long-term treatment.

In vitro EDL and diaphragm muscle characterization

In vitro characterization of intact muscle was performed as described previously (de Winter et al., 2020). The experimental protocols consisted of a full tetanus at 150 Hz (diaphragm) and 200 Hz (EDL) and a force-frequency protocol. For the force-frequency protocol, the muscle was stimulated with incremental stimulation frequencies (diaphragm: 1, 5, 10, 20, 40, 60, 80, 100, and 150 Hz; and EDL: 1, 5, 10, 20, 40, 60, 80, 100, 150, and 200 Hz). Data were discarded when stimulation at 150 Hz (diaphragm) or 200 Hz (EDL) rendered a force that was <90% of the force generated during the first maximal tetanic stimulation. Stimuli were applied with a train duration of 600 ms. The resting interval was 30 s between the stimulations at 1 and 10 Hz; 60 s after stimulation at 20 Hz; 90 s after stimulation at 30 Hz; and 120 s between stimulations at 60, 80, 100, 150, and 200 Hz. Then a fatigue protocol (80 contractions; 40 Hz; 2 s on and 1 s off) was performed. The peak force of each contraction was measured and normalized to muscle mass. A fatigue index corresponding to the ratio between the last five and the first five contractions was determined. After completion of the contractility measurements, the length and mass of the muscles were determined. Cross-sectional area (CSA; in mm^2) was calculated by dividing muscle mass (g) by muscle length (cm) multiplied by specific density (1.056 g/ml) × 100.

In vivo plantar flexor muscle measurements

Animal preparation: Mice were anesthetized and individually placed supine in a home-built cradle specially designed for the strictly non-invasive functional investigation of the left hind limb muscles as described previously (Gineste et al., 2013a). Force output measurements: Non-invasive transcutaneous electrical stimulation was first elicited with square-wave pulses (0.5-ms duration) on the plantar flexor muscles. The individual maximal stimulation intensity was determined by progressively increasing the stimulus intensity until there was no further peak twitch force increase. Plantar flexion force was assessed in response to stimulation trains delivered at 20 and 100 Hz (train duration = 750 ms). We chose those specific stimulation frequencies in vivo to match the relative force production we observed in vitro at 40 and 150 Hz. The resulting force was divided by the sum of GAS/plantaris + SOL muscle mass (in mN/mg). Then, a fatigue protocol (80 stimulations; 40 Hz; 1.5 s on and 6 s off) was performed. The peak force of each contraction was measured, normalized to muscle mass, and the corresponding values were averaged every five contractions. A fatigue index corresponding to the ratio between the last five and the first five contractions was determined.

Muscle fiber CSA analysis

Muscle fiber CSA was determined in the mid-belly region of GAS and EDL muscles and in a portion of the diaphragm muscle as previously described (Gineste et al., 2013b). Briefly, muscle serial transverse sections (10-µm thick) were obtained from each muscle and were immunostained with monoclonal antibodies against myosin heavy chain (MHC) isoforms (BA-F8 against MHC-1 and SC-71 against MHC-2A). The cryosections were incubated with a primary antibody for 1 h at 37°C, rinsed with PBS buffer, and incubated in a secondary rabbit anti-mouse antibody conjugated with peroxidase (DAKO) for 1 h at 37°C. After washing in PBS buffer, the stain was visualized by using a DAB (3,3′-diaminobenzidine) solution. Fibers negative for the two antibodies were considered type 2X or 2B. Images of the stained sections were captured from a light microscope (LeicaDMLS; ocular magnification: 10×, objective magnification: 10×, the numerical aperture of the objective lenses: 0.22) equipped with a camera (DFC450C; Leica), using the software LASV3.8. Fiber CSA was measured using the ImageJ 1.5 analysis software (Schneider et al., 2012) (NIH) and expressed in micrometers squared. Given the low number of fibers positive for antibodies against MHC-1 and MHC-2A, both in EDL and GAS muscles, CSA was assessed on the negative fibers (type 2X and 2B), which were the most prominent ones in both muscles. In the diaphragm muscle, CSA was measured without differentiation between fiber types.

Plethysmography analysis

Mice were placed in an unrestrained whole-body plethysmography chamber for 30 min for acclimatization. After acclimatization, tidal volume (VT), respiratory rate (RR), and minute ventilation (MV) were monitored for 15 min at room air. After 15 min, mice were exposed to a 5% CO_2 gas mixture for 30 min and monitored. After the 5% CO_2 exposure, mice were reexposed to room air for 15 min and monitored (de Winter et al., 2021). The data were analyzed by Buxco Finepointe Respirometry and Inhalation software (Data Science International). FinePointe software was used to acquire and analyze the respirometry data that were collected using the Buxco Small Animal Whole Body Plethysmography system. RR and VT were provided by the Finepointe software. MV was calculated as the product of RR and VT.

MHC composition analysis

Frozen EDL and GAS muscles were pulverized in a steel mortar with liquid nitrogen to obtain a powder that was immediately resuspended in Laemmli solution (Laemmli, 1970). The samples were incubated in ice for 20 min and finally spun at 18,000 *g* for 30 min. Protein concentration in the dissolved samples was determined with a protein assay kit (RC DC Biorad). About 10 µg of proteins for each sample was loaded on 8% SDS-PAGE polyacrylamide gels and the electrophoresis was run overnight at 250 V. Following a Coomassie stain, four bands corresponding to MHC isoforms were separated and their densitometric analysis was performed to assess the relative percentage of MHC isoforms (MHC-1, MHC-2A, MHC-2B, and MHC-2X) in the samples (Pellegrino et al., 2003).

Western blot analysis

Frozen GAS muscle samples were pulverized and immediately resuspended in a lysis buffer (20 mM Tris-HCl, 1% Triton X100, 10% glycerol, 150 mM NaCl, 5 mM EDTA, 100 mM NaF, and 2 mM NaPPi supplemented with 1× protease, phosphatase inhibitors [Sigma-Aldrich] and 1 mM PMSF). The homogenate obtained was kept on ice for 20 min and then centrifuged at 18,000 *g* for 20 min at 4°C. The supernatant was stored at −80°C until ready to use. Protein concentration was evaluated for each sample and equal amounts of muscle samples were loaded on gradient precast gels purchased from Bio-Rad (AnyKd). After the gel run, proteins were electro-transferred to PVDF membranes at 35 mA overnight. The membranes were incubated in 5% milk for 2 h, rinsed with TBST buffer (0.02 M Tris and 0.05 M NaCl, pH 7.4–7.6), and subsequently probed with specific primary antibodies (see below). Thereafter, the membranes were incubated in HRP-conjugated secondary antibodies. The protein bands were visualized by an enhanced chemiluminescence method in which luminol was excited by peroxidase in the presence of H_2O_2 (ECL Select, GE Healthcare). The content of each protein investigated was assessed by determining the brightness–area product of the protein band (Cannavino et al., 2015). Antibodies used were as follows: anti-rabbit GAPDH (catalog ab9484, 1:2,000; Abcam); anti-rabbit Catalase (catalog ab52477, 1:1,000; Abcam); anti-mouse SOD1 (catalog ab16831, 1:1,000; Abcam); anti-rabbit FIS1 (catalog ab71498, 1:1,000; Abcam); anti-rabbit p-DRP1$_{(ser616)}$ (catalog #3455, 1:1,000; Cell Signalling); anti-rabbit p-DRP1$_{(ser637)}$ (catalog #4867, 1:1,000; Cell Signalling); anti-rabbit DRP1 (catalog #8570, 1:3,000; Cell Signalling); anti-mouse MFN1 (catalog ab57602, 1:1,000; Abcam); anti-rabbit MFN2 (catalog ab50843, 1:1,000; Abcam); anti-rabbit OPA1 (catalog ab157457, 1:3,000; Abcam); anti-mouse IgG (catalog P026, 1:5,000; Dako North America Inc.); and anti-rabbit IgG (catalog #7074, 1:10,000; Cell Signalling).

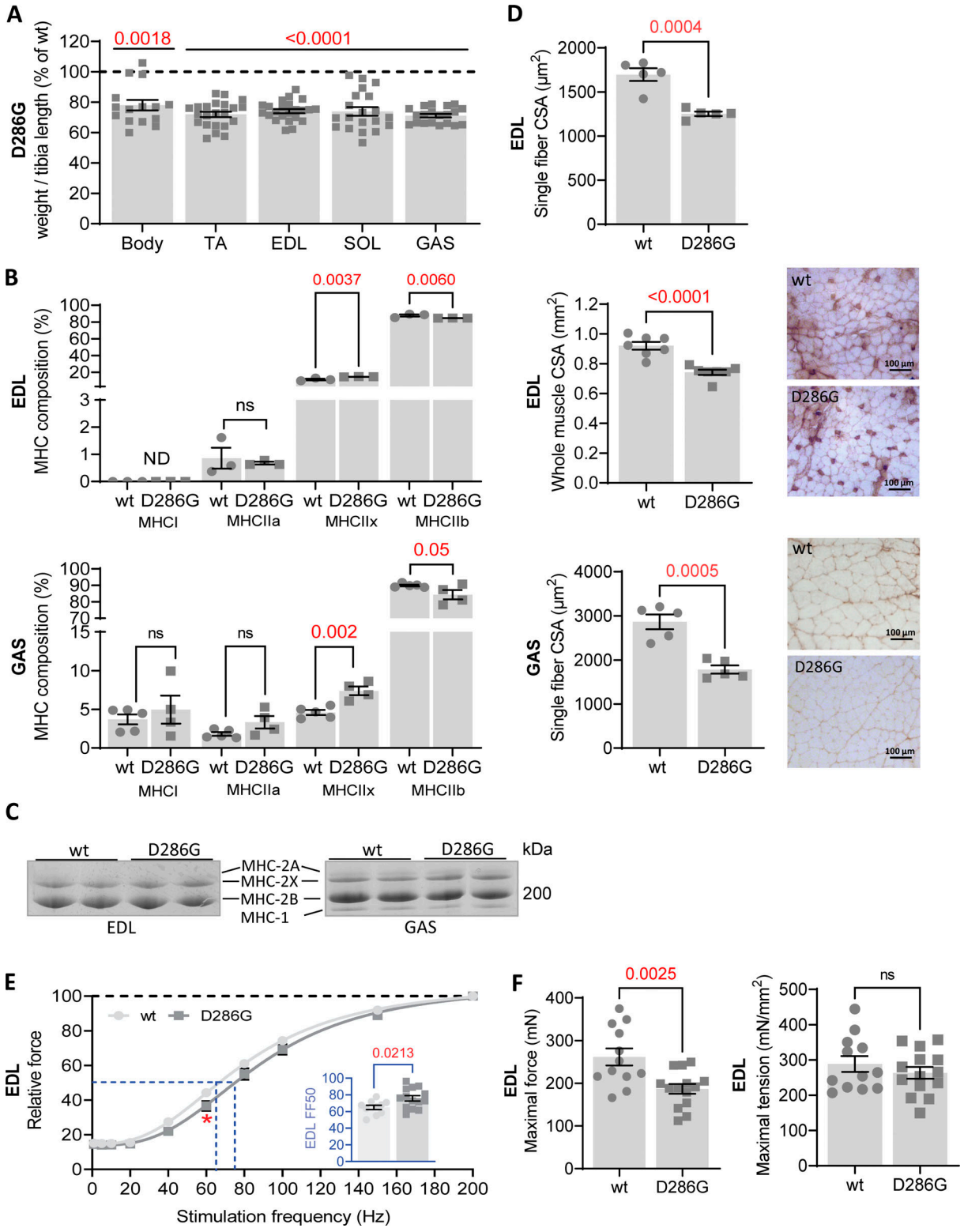

Figure 1. **Characterization of *Acta1*(D286G) mouse model. (A)** Body weight and wet muscle mass normalized over tibia length relative to the percentage of wild type values. **(B)** Top panel: MHC isoform composition of EDL muscle. Bottom panel: MHC isoform composition of GAS muscle. **(C)** Representative images of EDL and GAS MHC composition by SDS-PAGE gel. **(D)** Top panel: Whole EDL muscle CSA. Middle panel: CSA of EDL single fast fibers (2X and 2B). Right panels show immunostained representative cryosections (negative fibers are type 2X and 2B fibers). Bottom panel: GAS single 2X and 2B fast fibers CSA. Right panels show immunostained representative cryosections (negative fibers are type 2X and 2B fibers). Bottom panel: GAS single fiber CSA. **(E)** EDL force-frequency stimulation relation (inset shows FF50). **(F)** Left panel and right panel. EDL maximal force and maximal tension at 200 Hz stimulation frequency in wild type and *Acta*(D286G) mice. All data are presented as mean ± SEM. Statistical significance symbology: * ≤ 0.05, ** ≤ 0.01, *** ≤ 0.001. Source data are available for this figure: SourceData F1.

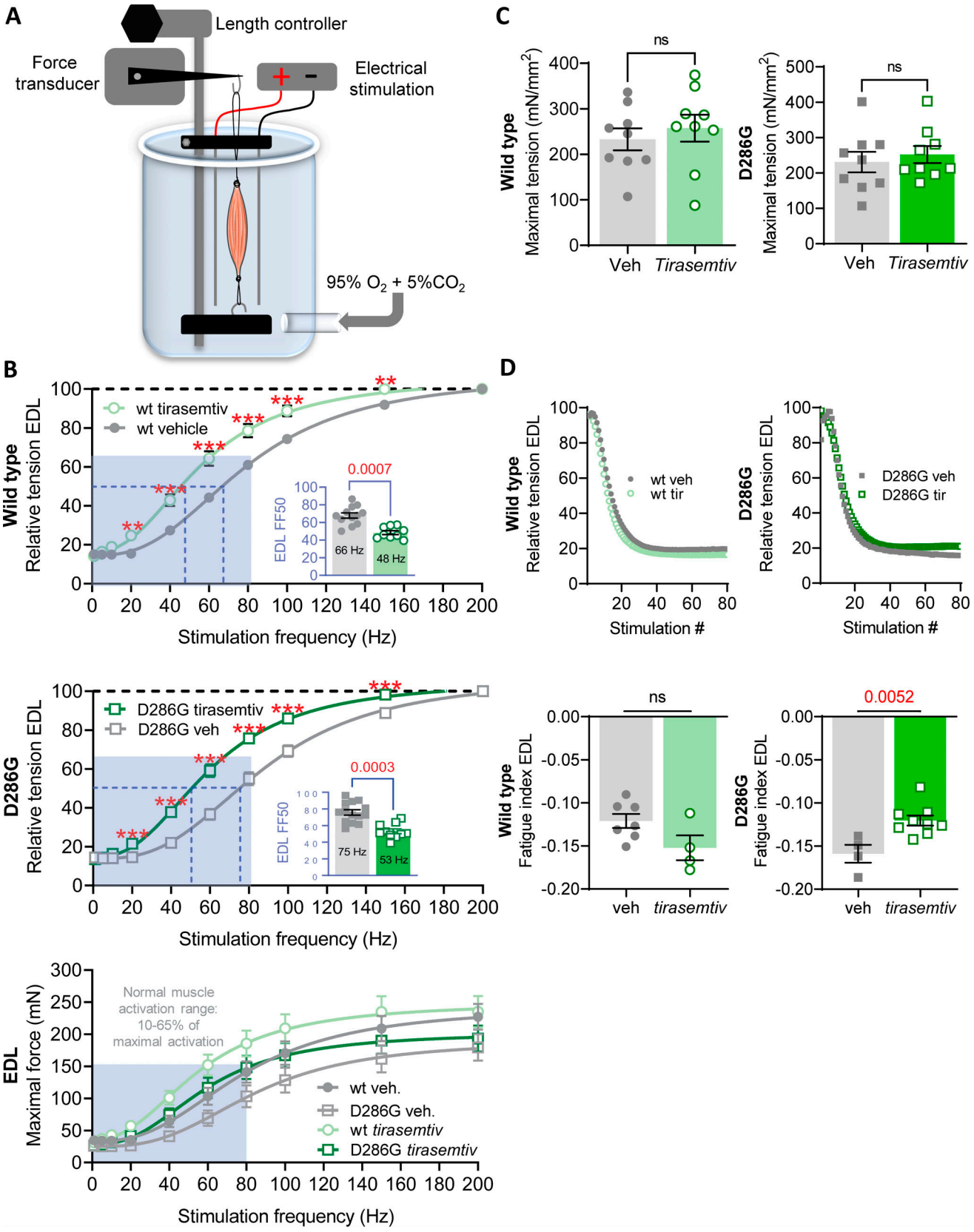

Figure 2. **In vitro muscle function after acute *tirasemtiv* treatment. (A)** Schematic representation of in vitro whole muscle intact mechanics system. **(B)** Top and middle panels: Relative force-frequency stimulation relation of EDL muscle in wild type and *Acta*(D286G) mice relative to their vehicle-treated group (insets show FF50). Bottom panel: Absolute forces during force frequency stimulation for all vehicle and *tirasemtiv*-treated groups. Blue shaded area in the force-frequency graphs represents the normal muscle activation level during daily life activities (10–65% [Tikkanen et al., 2013; Jasmin and Gardiner, 1987]).

Note that data points from vehicle-treated wild type *Acta1*(D286) mice are the same as those from baseline characterization in Fig. 1 D. **(C)** Left and right panels: The force at maximal stimulation (200 Hz) of wild type and *Acta*(D286G) relative to percentage of vehicle-treated mice. **(D)** Top left and right panels: EDL relative tension developed over a fatigue stimulation protocol in vehicle and *tirasemtiv*-treated wild-type and *Acta*(D286G) mice. Bottom left and right panels. Fatigue index during fatigue stimulation protocol in vehicle and *tirasemtiv*-treated wild type and *Acta*(D286G) mice. All data are presented as mean ± SEM. Statistical significance symbology: * ≤ 0.05, ** ≤ 0.01, *** ≤ 0.001.

Carbonylated protein analysis

Frozen GAS samples from each subject group were suspended in a lysis buffer (50 mM Tris-HCl pH 7.6, 250 mM NaCl, 5 mM EDTA protease inhibitor cocktail, and phosphatase inhibitor cocktail), left on ice for 20 min, and finally centrifuged at 18,000 *g* for 20 min at 4°C. Protein concentration was determined using the RC DC TM protein assay kit (Biorad product). The protein carbonylation level was detected using the OxyBlot TM Kit (Millipore), which provides reagents for sensitive immunodetection of carbonyl groups. Carbonyl groups in the protein side chains were derivatized to 2,4-dinitrophenylhydrazone (DNP) by reaction with 2,4-dinitrophenylhydrazine (DNPH). In detail, 10 µg of proteins for each muscle sample was denatured with SDS solution at a final concentration of 6%. DNPH solution was added to obtain the derivation; the reaction was stopped using a neutralization solution (90449; Millipore) after 10 min of incubation at room temperature. The DNP-derivatized protein samples were separated by polyacrylamide gel electrophoresis (Anykd Biorad gels) followed by Western blotting. Proteins were transferred to nitrocellulose membranes at 100 V for 2 h, stained with Ponceau Red (Sigma-Aldrich), and then scanned. The membranes were blocked by incubation with 3% bovine serum albumin for 1 h and then incubated with rabbit anti-DNP antibody overnight at 4°C and subsequently with a

Table 1. **In vitro EDL muscle mechanics—acute *tirasemtiv* treatment**

Frequency (Hz)	**1**	**5**	**10**	**20**	**40**	**60**	**80**	**100**	**150**	**200**	**# of mice**	**Age of mice in months**
***Acta1*(Wt)—vehicle**											9	8
Absolute force (mN)	34 ± 12	33 ± 11	33 ± 11	35 ± 11	64 ± 26	100 ± 40	136 ± 50	164 ± 55	203 ± 63	221 ± 65		
Normalized force (mN/mm^2)	35 ± 13	35 ± 13	34,5 ± 13	36 ± 13	66 ± 28	104 ± 43	141 ± 62	170 ± 62	214 ± 71	232 ± 7		
Relative force (% of maximum)	16 ± 1	15 ± 1	15 ± 1	16 ± 2	28 ± 6	44 ± 7	61 ± 6	75 ± 5	91 ± 3	100 ± 0.05		
Acta1*(Wt)—*tirasemtiv											9	8
Absolute force (mN)	31 ± 13	37 ± 7	44 ± 10	58 ± 16	103 ± 34[a]	156 ± 50[a]	193 ± 61[a]	216 ± 67[a]	242 ± 74[a]	232 ± 80		
Normalized force (mN/mm^2)	32 ± 15	39 ± 10	45 ± 13	60 ± 19[a]	106 ± 37[a]	161 ± 57[a]	199 ± 69	222 ± 77	250 ± 85	237 ± 87		
Relative force (% of maximum)	13 ± 2	16 ± 2	18 ± 2	24 ± 3[a]	42 ± 6[a]	63 ± 7[a]	78 ± 4[a]	87 ± 2[a]	98 ± 2[a]	100 ± 0.2		
***Acta1*(D286G)—vehicle**											9	8
Absolute force (mN)	24 ± 9[b]	24 ± 9[b]	24 ± 9[b]	25 ± 10[b]	40 ± 19[b]	66 ± 33[b]	97 ± 47	121 ± 54	152 ± 60	168 ± 60		
Normalized force (mN/mm^2)	32 ± 12	31 ± 12	31 ± 12	33 ± 13	52 ± 26	87 ± 45	129 ± 63	159 ± 71	200 ± 79	221 ± 79		
Relative force (% of maximum)	14 ± 2	14 ± 2	14 ± 2	15 ± 2	22 ± 6[b]	37 ± 9[b]	55 ± 10[b]	69 ± 5[b]	89 ± 3	100 ± 0.0		
Acta1*(D286G)—*tirasemtiv											9	8
Absolute force (mN)	26 ± 13	28 ± 10	32 ± 12	43 ± 15	76 ± 31[a]	119 ± 48[a]	151 ± 55[a]	171 ± 58[a]	194 ± 61[a]	197 ± 62		
Normalized force (mN/mm^2)	38 ± 11	39.2 ± 12	44.6 ± 13	58.6 ± 18	104.7 ± 39[a]	163.9 ± 59[a]	206.5 ± 67[a]	231.7 ± 71[a]	261.3 ± 74[a]	264.3 ± 76		
Relative force (% of maximum)	13 ± 2	14 ± 3	16 ± 3	21 ± 7[a]	37 ± 9[a]	58 ± 8[a]	74 ± 6[a]	85 ± 3[a]	97 ± 1[a]	100 ± 1.3		

[a]*Tirasemtiv* versus vehicle ($P < 0.05$).
[b]Acta1(D286G) versus Acta1(wt) ($P < 0.05$).

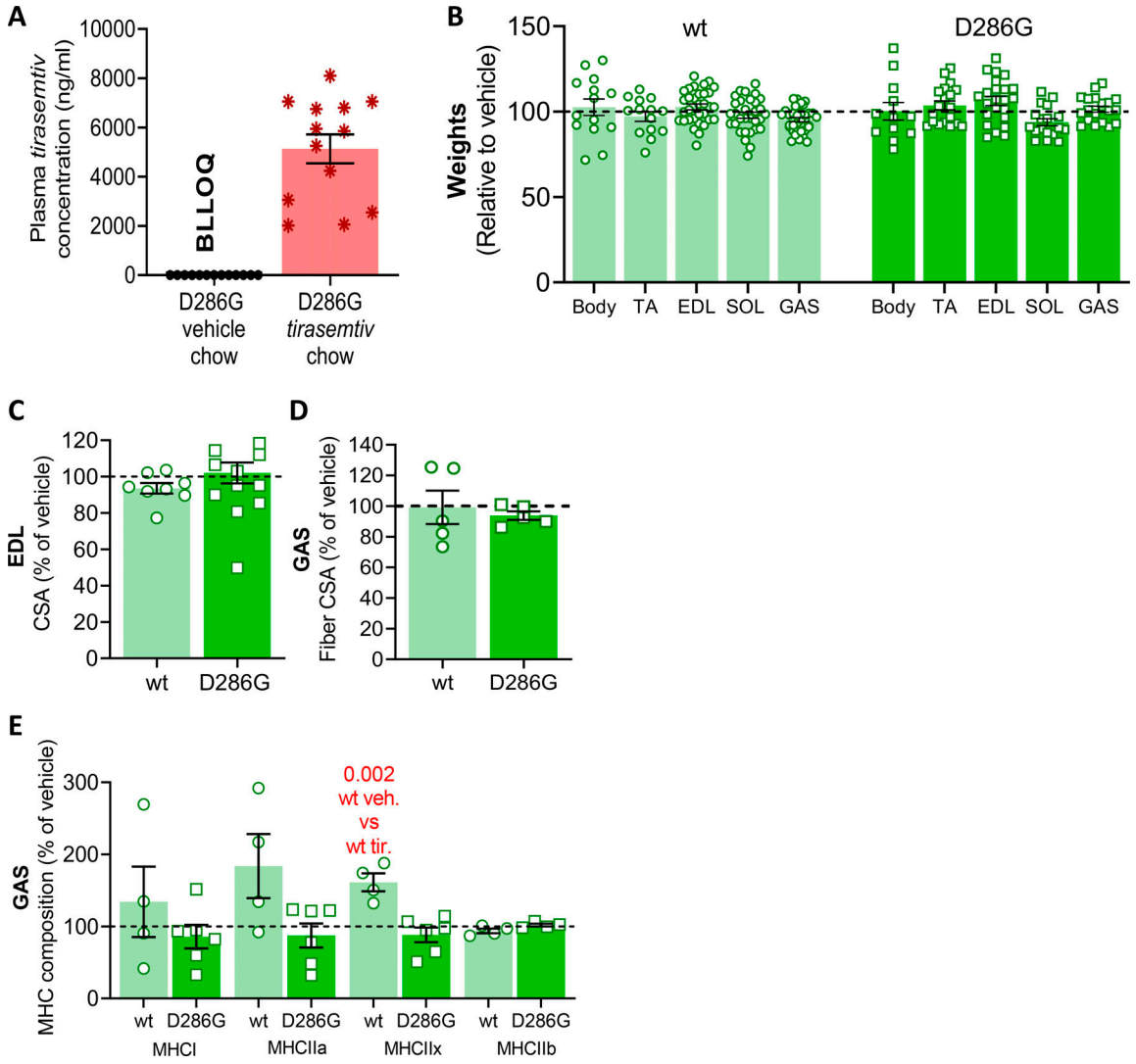

Figure 3. **Long-term effects of *tirasemtiv* on muscle mass and fiber type. (A)** Plasma *tirasemtiv* concentration level after long-term administration of vehicle chow and *tirasmtiv* chow in mice (BLLOQ = below lower level of quantification). **(B)** Effect of long-term *tirasemtiv* administration on body and wet muscle mass (right and left leg muscles included), normalized over tibia length relative to vehicle-treated wild type and *Acta*(D286G) mice. **(C)** Effect of long-term *tirasemtiv* administration on EDL whole muscle CSA. **(D)** Effect of long-term *tirasemtiv* administration on CSA of the most prominent GAS fiber types (2X and 2B). **(E)** Effect of long-term *tirasemtiv* administration on fiber type composition in GAS muscle. All data are presented relative to the data from the vehicle-treated wild type or vehicle-treated *Acta*(D286G) group. All data are presented as mean ± SEM.

horseradish peroxidase-antibody conjugate (goat anti-rabbit IgG). The positive bands were visualized by using a chemiluminescent reagent (ECL advance as described previously [Cannavino et al., 2015]). The total protein carbonylation level and the MHC carbonylation level were analyzed quantitatively by comparison of the signal intensity of immune-positive proteins normalized on the total protein amount loaded on gels (ponceau staining signal) (Cannavino et al., 2015).

Gene expression analysis

Total RNA was extracted from GAS muscles using an SV Total RNA isolation kit (Promega). The RNA concentration was measured using a Nano Drop instrument (Thermo Fisher Scientific) and 400 ng was used to generate cDNA with SuperScript III reverse transcriptase (Invitrogen). The cDNA was analyzed by quantitative RT-PCR (AB7500; Applied Biosystems) using a SYBR Green PCR kit (Applied Biosystems), and the data were normalized to *Gapdh* content. Oligonucleotide primers were provided by Sigma-Aldrich and were *MuRF-1* (FP: 5′-ACCTGC TGGTGGAAAACATC-3′, RP: 5′-ACCTGCTGGTGGAAAACATC-3′) and *Atrogin-1* (FP: 5′-GCAAACACTGCCACATTCTCTC-3′, RP: 5′-CTTGAGGGGAAAGTGAGACG-3′). Differentially expressed genes were determined using a default threshold of 0.6. The difference between Ct (cycle threshold) values was calculated for each mRNA by taking the mean Ct of duplicate reactions and subtracting the mean Ct of duplicate reactions for the reference RNA measured on an aliquot from the same RT reaction (ΔCt = Ct target gene − Ct reference gene). All samples were then normalized to the ΔCt value of a calibrator sample to obtain a ΔΔCt value (ΔCt target − ΔCt calibrator) (comparative method) (Cannavino et al., 2015).

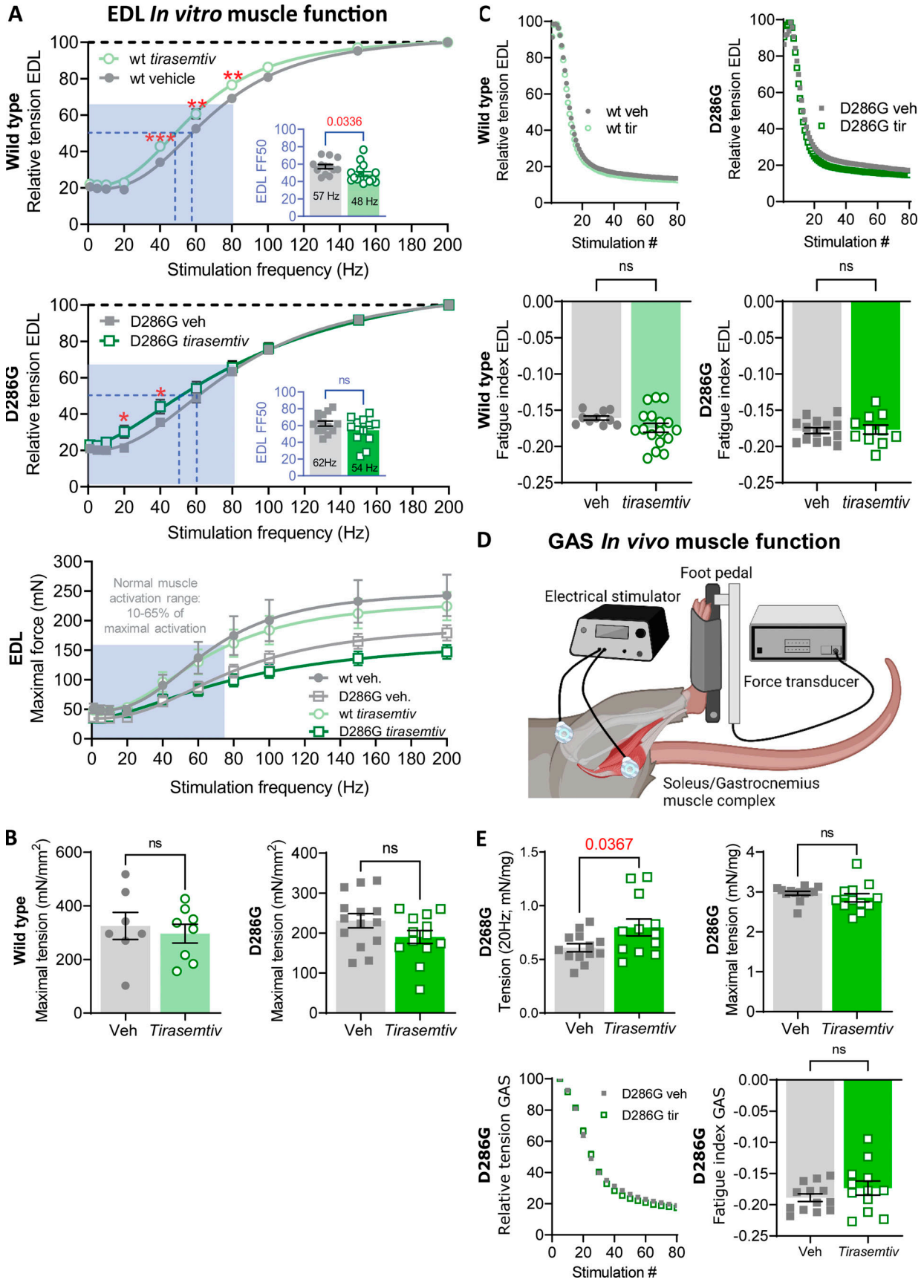

Figure 4. **In vitro and in vivo muscle function after long-term *tirasemtiv* treatment. (A)** Top and middle panels: Force-frequency stimulation relation of EDL muscle in wild type and *Acta*(D286G) mice relative to their vehicle-treated group (insets show FF50). Bottom panel: Absolute forces during at various

stimulation frequencies for all vehicle and *tirasemtiv*-treated groups. The blue shaded area in the force-frequency graphs represents the normal muscle activation level during daily life activities (10–65% [Tikkanen et al., 2013; Jasmin and Gardiner, 1987]). **(B)** Left and right panels: The maximal tension at 200 Hz stimulation frequency in wild type and *Acta*(D286G) mice relative to their vehicle-treated group. **(C)** Top left and right panels: EDL relative tension developed over a fatigue stimulation protocol in vehicle and *tirasemtiv* treated wild type and *Acta*(D286G) mice. Bottom left and right panels: Fatigue index during fatigue stimulation protocol in vehicle and *tirasemtiv*-treated wild type and *Acta*(D286G) mice. **(D)** Schematic representation of in vivo GAS force measurements. **(E)** Top left panel: GAS tension at 20 Hz stimulation in *Acta*(D286G) GAS muscle relative to its vehicle-treated group. Top right panel: GAS tension at maximal stimulation frequency (150 Hz) in *Acta*(D286G) GAS muscle relative to its vehicle-treated group. Bottom left panel: relative tension developed over a fatigue stimulation protocol in *tirasemtiv*-treated *Acta*(D286G) mice. Bottom right panel: Fatigue index during fatigue stimulation protocol in *tirasemtiv*-treated *Acta*(D286G) mice. All data are presented as mean ± SEM. Statistical significance. Symbology: * ≤ 0.05, ** ≤ 0.01, *** ≤ 0.001.

Statistics

Data are presented as mean ± standard error of the mean. For mouse model characterization and long-term *tirasemtiv* effect data analysis, an unpaired *t* test or two-way ANOVA followed by Sidak's multiple comparison test (for force-frequency data and baseline MHC composition) was used. For acute *tirasemtiv* effect data analysis, paired *t* test or repeated measures two-way ANOVA followed by Sidak's multiple comparison test (for force-frequency data) was used. All data analysis was performed with GraphPad Prism 9 software (version 9.5.1 [733]). A probability value <0.05 was considered statistically significant.

Online supplemental material

Fig. S1 describes the effect of long-term *tirasemtiv* administration on protein expression of muscle mitochondrial dynamic markers. All mitochondrial markers were measured in GAS muscles of wild type and *Acta1*(D286G) *tirasemtiv*- and vehicle-treated mice.

Table 2. **In vitro EDL muscle mechanics—long-term *tirasemtiv* treatment**

Frequency (Hz)	1	5	10	20	40	60	80	100	150	200	# of mice	Age of mice in months
***Acta1*(Wt)—vehicle**											7	9
Absolute force (mN)	52 ± 22	50 ± 21	49 ± 20	49 ± 21	92 ± 48	140 ± 73	178 ± 89	204 ± 95	237 ± 98	248 ± 95		
Normalized force (mN/mm^2)	72 ± 30	68 ± 28	67 ± 28	67 ± 28	127 ± 57	192 ± 100	244 ± 122	280 ± 130	325 ± 134	340 ± 130		
Relative force (% of maximum)	21 ± 2	20 ± 2	19 ± 2	19 ± 2	34 ± 7	53 ± 9	69 ± 8	81 ± 6	95 ± 3	100 ± 0.0		
Acta1*(Wt)—*tirasemtiv											8	9
Absolute force (mN)	49 ± 16	48 ± 15	49 ± 15	54 ± 18	98 ± 48	133 ± 61	165 ± 67	187 ± 70	213 ± 72	229 ± 69		
Normalized force (mN/mm^2)	68 ± 21	66 ± 21	67 ± 21	74 ± 25	134 ± 66	182 ± 84	226 ± 92	260 ± 96	297 ± 99	314 ± 95		
Relative force (% of maximum)	22 ± 2	22 ± 2	21 ± 27	23 ± 2	43 ± 10[a]	61 ± 11[a]	77 ± 8[a]	86 ± 6	97 ± 2	100 ± 0.1		
***Acta1*(D286G)—vehicle**											14	9
Absolute force (mN)	37 ± 11	36 ± 11	35 ± 11	37 ± 12	64 ± 26	89 ± 35	117 ± 42	139 ± 45	168 ± 48	183 ± 49		
Normalized force (mN/mm^2)	51 ± 16	49 ± 15	49 ± 15	51 ± 16	87 ± 36	123 ± 48	160 ± 58	190 ± 62	231 ± 66	251 ± 68		
Relative force (% of maximum)	21 ± 3	20 ± 3	20 ± 3	22 ± 4	34 ± 8	49 ± 10	63 ± 9	75 ± 8	92 ± 4	100 ± 0.0		
***Acta1*(D286G)—*tirasemtiv*[b]**											12	9
Absolute force (mN)	36 ± 12	35 ± 13	38 ± 15	45 ± 21	68 ± 31	84 ± 36	101 ± 39	116 ± 41	139 ± 43	150 ± 43		
Normalized force (mN/mm^2)	49 ± 17	48 ± 17	52 ± 21	62 ± 29	93 ± 42	115 ± 49	139 ± 53	159 ± 56	190 ± 58	206 ± 59		
Relative force (% of maximum)	23 ± 2	23 ± 3	25 ± 5	30 ± 12[a]	44 ± 13[a]	54 ± 13	66 ± 12	76 ± 10	92 ± 4	100 ± 0.0		

[a]Tirasemtiv versus vehicle ($P < 0.05$).
[b]Acta1(D286G) versus Acta1(wt) ($P < 0.05$).

Table 3. **In vivo *plantar flexor* muscle mechanics—long-term *tirasemtiv* treatment**

Frequency (Hz)	20	100	# of mice	Age of mice in months
***Acta1*(D286G)—vehicle**			13	9
Absolute force (mN)	69 ± 17	334 ± 31		
Normalized force (mN/mg)	0.6 ± 0.1	3.0 ± 0.2		
Relative force (% of maximum)	21 ± 4.6	100 ± 6.1		
Acta1*(D286G)—*Tirasemtiv			12	9
Absolute force (mN)	83 ± 31	293[a] ± 32		
Normalized force (mN/mg)	0.8[a] ± 0.3	2.9 ± 0.4		
Relative force (% of maximum)	29 ± 9.3[a]	100 ± 13		

[a]*Tirasemtiv* versus Vehicle ($P < 0.5$).

Results

Characterization of *Acta1*(D286G) mouse skeletal muscles

In line with previous work (Ravenscroft et al., 2011a), homozygous *Acta1*(D286G) mice had lower whole-body weight as well as lower hind limb muscle mass when compared with wild type mice (Fig. 1 A). Since *tirasemtiv* targets exclusively fast-twitch muscle fibers, we determined the morphological and functional characteristics of the fast glycolytic EDL and GAS muscles. Both EDL and GAS muscles of *Acta1*(D286G) mice had a significantly higher proportion of MHC type IIx and a significantly lower proportion of type MHC IIb compared with wild type mice. The proportion of MHC type I and IIa was comparable between groups (Fig. 1 B, top and bottom panels). Representative images of EDL and GAS MHC fiber type using SDS-PAGE polyacrylamide gels are shown in Fig. 1 C, bottom panel.

Muscle atrophy is often observed in NEM. Since we observed lower muscle mass in TA, SOL, EDL, and GAS in *Acta1*(D286G) mice, we measured EDL physiological CSA and CSA of the most prominent fiber types, 2X and 2B, of both EDL and GAS muscle to assess atrophy. Whole EDL CSA and single fiber CSA of EDL and GAS were significantly lower in *Acta1*(D286G) mice (Fig. 1 D). Since muscle atrophy is usually associated with a decrease in force production, we measured the contractile parameters of EDL at incremental stimulation frequencies, which reflect muscle function during different daily life activities (Tikkanen et al., 2013; Jasmin and Gardiner, 1987). Relative forces of EDL at submaximal stimulation frequencies (60 Hz) were significantly lower in *Acta1*(D286G) mice (Fig. 1 D). As a consequence, the FF50, which represents the stimulation frequency required to generate 50% of maximal force, was significantly higher in *Acta1*(D286G) mice (Fig. 1 E; inset). The maximal force (200 Hz) of EDL was significantly lower in *Acta1*(D286G) mice; however, the maximal normalized force (i.e., tension) was comparable with wild type (Fig. 1 F). Thus, muscles of *Acta1*(D286G) mice have atrophy and a reduced maximal absolute force in addition to lower relative force in response to submaximal stimulation frequencies.

Acute effect of *tirasemtiv* on skeletal muscle function

We first investigated the acute effect of *tirasemtiv* treatment on EDL muscles in vitro. EDL muscles were isolated and mounted in an in vitro whole muscle intact mechanics system and electrically stimulated (schematic representation, Fig. 2 A). Wild type and *Acta1*(D286G) EDL muscles were exposed to 3 µM of *tirasemtiv*. This dose was chosen based on previous work that showed maximal contractility gain without impairing muscle relaxation kinetics (de Winter et al., 2021). *Tirasemtiv* exposure resulted in a leftward shift of the force-frequency curve with significantly higher relative tension at stimulation frequencies of 20, 40, 60, 80, 100, and 150 Hz in wild type and in *Acta1*(D286G) mice (Fig. 2 B; top and middle panels). The FF50 was significantly lower in wild type and *Acta1*(D286G) *tirasemtiv*-treated muscles (Fig. 2 B, top and middle panel insets). Fig. 2 B, bottom panel, shows tensions generated by EDL during the force-frequency protocol for all groups and experimental conditions. As anticipated, *tirasemtiv* did not affect the maximal tension in wild type and *Acta1*(D286G) EDL muscles (Fig. 2 C). Acute *tirasemtiv* forces are shown in Table 1. Furthermore, we assessed the effect of *tirasemtiv* on the fatigability of EDL. We repeatedly stimulated wild type and *Acta1*(D286G) EDL muscles (Fig. 2 D; top row) and determined the fatigue index. *Acta1*(D286G) EDL muscles exposed to *tirasemtiv* showed significantly higher resistance to fatigue development (Fig. 2 D; bottom right panel). No effect was observed on wild type muscles (Fig. 2 D, bottom left panel). Thus, acute *tirasemtiv* treatment increased force production at submaximal stimulation frequencies and increased the resistance to fatigue in *Acta1*(D286G) EDL muscles.

Effect of long-term *tirasemtiv* treatment on skeletal muscle morphology and contractility

To investigate the long-term effects of *tirasemtiv* on contractility of EDL (in vitro) and GAS (in vivo), wild type and *Acta1*(D286G) mice were fed *tirasemtiv*-enriched chow for 4 wk. After 4 wk of treatment, plasma levels of *tirasemtiv* ranged from 2,020 to 8,100 ng/ml. No *tirasemtiv* was detected in the plasma of mice fed standard chow (Fig. 3 A). *Tirasemtiv* treatment did not result in any significant body or muscle mass changes in wild type and *Acta1*(D286G) mice compared with vehicle-treated mice (Fig. 3 B). Additionally, long-term *tirasemtiv* treatment did not affect whole EDL CSA or GAS single fiber CSA (Fig. 3, C and D). We then assessed GAS fiber type composition. GAS of *tirasemtiv*-treated wild type mice had a significantly higher percentage of MHC type 2X fibers as compared to vehicle-treated mice (Fig. 3 E). We did not observe significant changes in fiber type composition in *tirasemtiv*-treated *Acta1*(D286G) mice. Since we observed a positive ionotropic effect of acute *tirasemtiv* treatment on EDL contractility, we next evaluated the long-term effect of *tirasemtiv* on in vitro EDL. Note that after EDL isolation and prior to the contractility assay, to wash out *tirasemtiv* and rule out acute effects on contractility, EDL was bathed for ∼20 min in

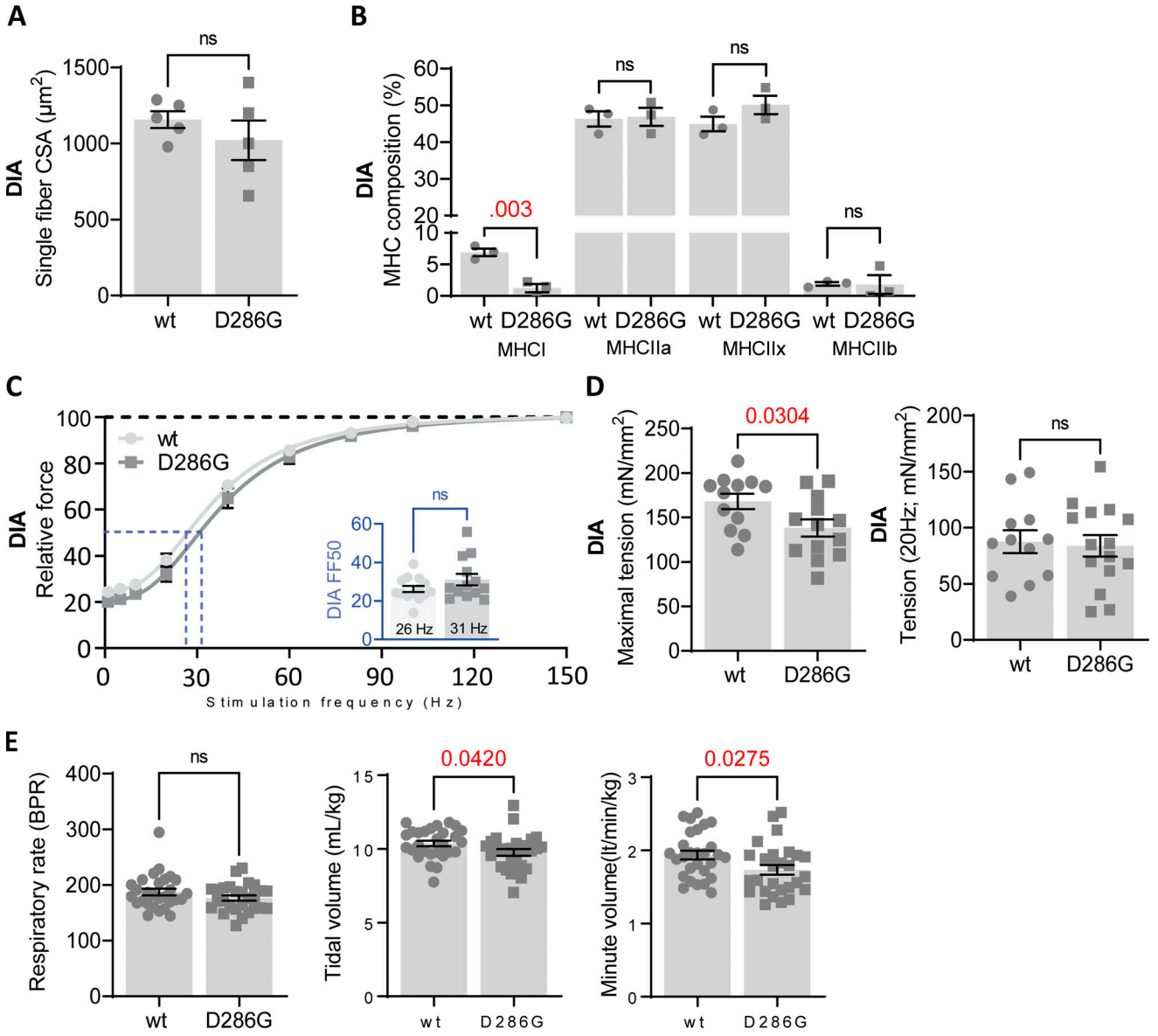

Figure 5. **Diaphragm muscle characterization of *Acta1*(D286G) mouse model. (A)** Diaphragm single fiber CSA. **(B)** MHC isoform composition in the diaphragm muscle as determined by SDS-PAGE. **(C)** Force-frequency stimulation relation of diaphragm muscle strips in wild type and *Acta*(D286G) mice (inset shows FF50). **(D)** Left panel: Maximal tension at 150 Hz stimulation frequency in wild type and *Acta*(D286G) diaphragm strips. Right panel: Tension at 20 Hz stimulation in wild type and *Acta*(D286G) diaphragm strips. **(E)** Left, middle, and right panel: Respiratory rate, tidal volume, and minute volume respectively, in wild type and *Acta*(D286G) mice measured by whole-body plethysmography.

tirasemtiv-free Ringer solution according to previous work (de Winter et al., 2021; Hwee et al., 2014). Similar to the observed acute effect of *tirasemtiv* in EDL muscles, long-term *tirasemtiv* treatment resulted in a leftward shift of the force-frequency curve with significantly higher relative tensions at stimulation frequencies of 40, 60, and 80 Hz in wild type and 20 and 40 Hz in *Acta1*(D286G) mice (Fig. 4 A; top and middle panel). The FF50 was significantly lower in the wild type but not in *Acta1*(D286G) *tirasemtiv*-treated muscles (Fig. 4 A; top and middle panel, insets). Fig. 4 A, bottom panel, shows tensions generated by EDL during the force-frequency protocol for all groups and experimental conditions. No effect of *tirasemtiv* was observed at maximal stimulation frequencies (200 Hz) in wild type mice and *Acta1*(D286G) EDL muscles (Fig. 4 B; left and right panel, accordingly). Furthermore, long-term *tirasemtiv* treatment did not have an effect on EDL fatigability in both wild type and *Acta1*(D286G) mice (Fig. 4 C). Long-term in vitro *tirasemtiv* force values are shown in Table 2.

Next, we evaluated the in vivo effect of long-term *tirasemtiv* administration on GAS contractile function. Whole GAS function was evaluated in vivo using an experimental setup previously described (Giannesini et al., 2010) (schematic representation, Fig. 4 D). Note that during these measurements, GAS muscles were not washed in *tirasemtiv*-free ringer solution as was done with EDL muscles. Similar to what we observed in EDL, at submaximal stimulation frequency, *Acta1*(D286G) *tirasemtiv*-

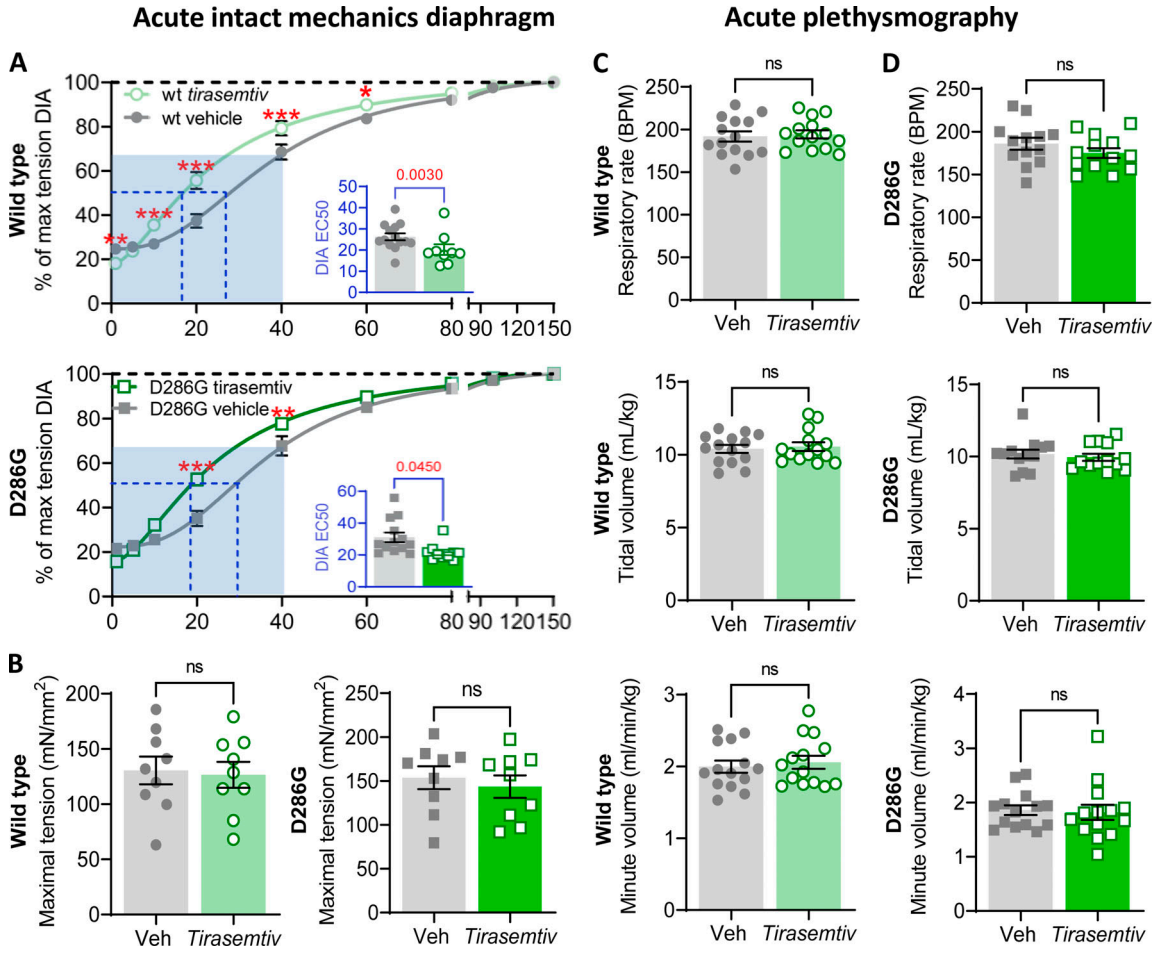

Figure 6. **Effect of acute *tirasemtiv* administration on respiratory muscle function in wild type and *Acta1*(D286G) mice. (A)** Top and bottom panels: Force-frequency stimulation relation of diaphragm muscle strips in wild type and *Acta*(D286G) mice relative to their vehicle-treated group (inset shows FF50). **(B)** Left and right panel: The maximal tension at 200 Hz stimulation frequency in wild type and *Acta*(D286G) mice relative to their vehicle-treated group. **(C and D)** Top, middle, and bottom panels: Respiratory rate, tidal volume, and minute volume respectively, in wild type and *Acta*(D286G) mice measured by whole-body plethysmography. Statistical significance symbology: * ≤ 0.05, ** ≤ 0.01, *** ≤ 0.001.

treated mice produced significantly higher tension as compared to vehicle-treated mice (Fig. 4 E; top left panel). No significant differences were observed in tension at maximal stimulation frequency (Fig. 4 E; top right panel) or GAS response to fatigue after *tirasemtiv* treatment (Fig. 4 E, bottom left and right panel). The long-term in vivo *tirasemtiv* force values are shown in Table 3.

Thus, these data indicate that long-term *tirasemtiv* administration enhances submaximal muscle tension in both EDL and GAS muscles of *Acta1*(D286G) mice. The sustained in vitro effect of *tirasemtiv* on EDL muscles after removal by washing suggests that in addition to its direct effect, long-term *tirasemtiv* treatment may induce structural changes within the muscle that improve force generation.

Characterization of *Acta1*(D286G) mouse diaphragm muscle function

Respiratory dysfunction is often observed in NEM patients. Thus, we investigated the effect of *tirasemtiv* administration on respiratory function and diaphragm contractility in vitro and in vivo. First, we characterized diaphragm morphology and function in untreated wild type and *Acta1*(D286G) mice. In contrast to EDL and GAS, we did not observe significant differences in diaphragm fiber CSA between wild type and *Acta1*(D286G) mice (Fig. 5 A). We then characterized the MHC composition of diaphragm muscle strips. *Acta1*(D286G) and wild type mouse diaphragm were predominantly composed of MHC type 2A and 2X (~90%). The diaphragm of *Acta1*(D286G) mice had a significantly lower percentage of MHC type I compared with wild type mice (1.2 versus 6.9%, respectively, Fig. 5 B). Next, we characterized diaphragm contractility in vitro. No significant changes were observed in the force-frequency relation and FF50 between both groups (Fig. 5 C). Maximal tension was significantly reduced in diaphragm strips of *Acta1*(D286G) mice compared with wild type (Fig. 5 D, left panel); however, unlike EDL and GAS, no changes were observed at submaximal stimulation frequencies (Fig. 5 D, right panel). We then characterized in vivo respiratory function in wild type and *Acta1*(D286G) mice using whole-body plethysmography. RR was comparable between groups (Fig. 5 E; left panel); however, tidal volume (VT; the volume of air moved in and out the lungs during

Table 4. **In vitro diaphragm muscle mechanics—acute *tirasemtiv* treatment**

Frequency (Hz)	1	5	10	20	40	60	80	100	150	# of mice	Age of mice in months
***Acta1*(Wt) vehicle**										9	8
Absolute force (mN)	20 ± 8	21 ± 9	23 ± 10	32 ± 16	59 ± 23	71 ± 26	76 ± 27	80 ± 28	82 ± 28		
Normalized force (mN/mm^2)	32 ± 10	33 ± 10	36 ± 12	51 ± 22	94 ± 32	113 ± 35	122 ± 36	128 ± 37	131 ± 39		
Relative force (% of maximum)	24 ± 5	26 ± 5	28 ± 6	38 ± 10	71 ± 9	86 ± 6	93 ± 3	98 ± 2	99 ± 1		
Acta1*(Wt)—*tirasemtiv										9	8
Absolute force (mN)	14 ± 7	18 ± 80	26 ± 10	42 ± 18	61 ± 27	69 ± 30	73 ± 32	75 ± 32	76 ± 33		
Normalized force (mN/mm^2)	24 ± 10[a]	31 ± 12	46 ± 14[a]	73 ± 24[a]	104 ± 33[a]	117 ± 35	123 ± 36	127 ± 36	129 ± 36		
Relative force (% of maximum)	18[a] ± 5	24 ± 5	35[a] ± 8	56[a] ± 11[a]	79[a] ± 10	90[a] ± 7	95 ± 4	98 ± 2	100 ± 0.2		
***Acta1*(D286G)—vehicle**										10	8
Absolute force (mN)	15 ± 7	16 ± 7	18 ± 9	24 ± 13	50 ± 24	63 ± 24	69 ± 24	72 ± 25	75 ± 25		
Normalized force (mN/mm^2)	31 ± 10	30 ± 11	34 ± 14	46 ± 23	95 ± 44	120 ± 47	133 ± 49	140 ± 51	145 ± 52		
Relative force (% of maximum)	20 ± 7	21 ± 7	34 ± 8	32 ± 12	65 ± 16	83 ± 10	92 ± 7	96 ± 3	100 ± 0.07		
***Acta1*(D286G)—*tirasemtiv*[b]**										10	8
Absolute force (mN)	11 ± 6	14 ± 6	21 ± 9	35 ± 15	52 ± 22	62 ± 24	64 ± 24	65 ± 25	67 ± 25		
Normalized force (mN/mm^2)	24 ± 8	31 ± 8	48 ± 12	79 ± 19	116 ± 27	134 ± 27	14 ± 26	146 ± 26	149 ± 26		
Relative force (% of maximum)	16 ± 3[a]	21 ± 4	32 ± 6[a]	53 ± 9[a]	78 ± 8	90 ± 4	96 ± 2	98 ± 1	100 ± 0.0		

[a]*Tirasemtiv* versus vehicle ($P < 0.05$).
[b]Acta1(D286G) versus Acta1(wt) ($P < 0.05$).

one respiratory cycle) and minute volume (VE; the product of RR and VT), were significantly reduced in *Acta1*(D286G) mice (Fig. 5 E; middle and right panel). Thus, the diaphragm of *Acta1*(D286G) mice shows contractile weakness and impaired respiratory function.

Acute effect of *tirasemtiv* on respiratory function

Next, we tested the acute effect of *tirasemtiv* on diaphragm contractility in vitro and on respiratory function in vivo. Acute *tirasemtiv* treatment resulted in a leftward shift in the force-frequency relation with significantly higher force production

Table 5. **Plethysmography—acute *tirasemtiv* treatment**

	Vehicle		*Tirasemtiv*			
	Rest	5% CO_2	Rest	5% CO_2	# of mice	Age of mice in months
***Acta1*(wt)[a]**					14	8
Respiratory rate (per minute)	191 ± 23	182 ± 37	194 ± 18	179 ± 23		
Tidal volume (ml/kg)	10.4 ± 1	10.3 ± 1	10.6 ± 1.1	10.1 ± 0.8		
Minute volume (ml/kg/minute)	1,997 ± 318	1,876 ± 317	2,057 ± 338	1,690 ± 568		
***Acta1*(D286G)[b]**					14	8
Respiratory rate (per minute)	184 ± 25	168 ± 22	175 ± 21	164 ± 31		
Tidal volume (ml/kg)	10.1 ± 1.1	9.4 ± 1.2	9.9 ± 0.9	9.6 ± 1.2		
Minute volume (ml/kg/minute)	1,859 ± 338	1,485 ± 519	1,766 ± 307	1,504 ± 598		

[a]*Tirasemtiv* versus vehicle ($P < 0.05$).
[b]Acta1(D286G) versus Acta1(wt) ($P < 0.05$).

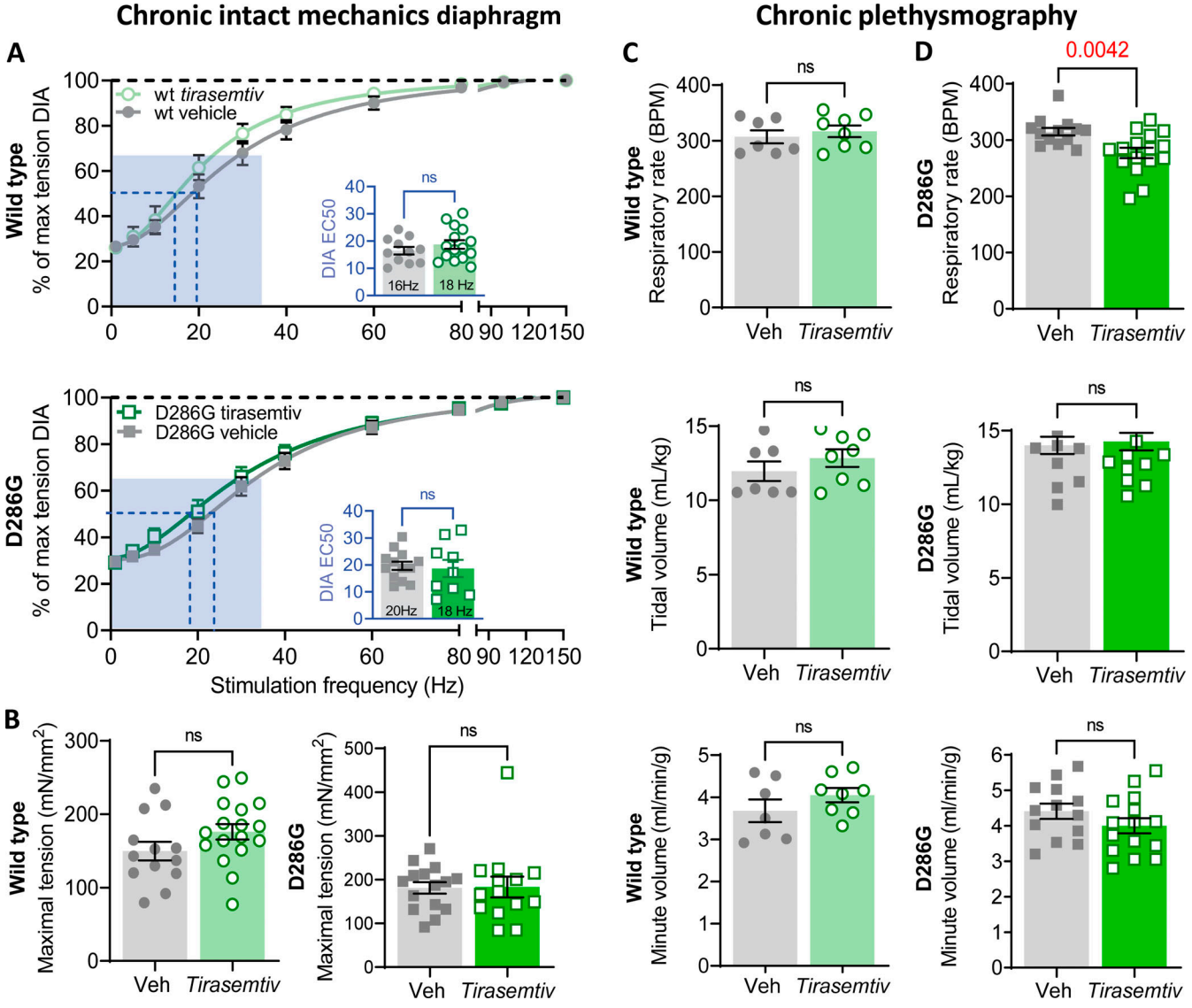

Figure 7. **Effect of long-term *tirasemtiv* administration on respiratory muscle function in wild type and *Acta1*(D286G) mice. (A)** Top and bottom panels: Force-frequency stimulation relation of DIA muscle strips in wild type and *Acta*(D286G) mice relative to their vehicle-treated group (inset shows FF50). **(B)** Left and right panel: The maximal tension at 200 Hz stimulation frequency in wild type and *Acta*(D286G) mice relative to their vehicle-treated group. **(C and D)** Top, middle, and bottom panels: Respiratory rate, tidal volume, and minute volume after 5% CO_2 exposure respectively, in wild type and *Acta*(D286G) mice measured by whole-body plethysmography. Statistical significance symbology: * ≤ 0.05, ** ≤ 0.01, *** ≤ 0.001.

at submaximal stimulation frequencies of 1, 10, 20, 40, and 60 Hz for wild type and 20 and 40 Hz for *Acta1*(D286G) mice (Fig. 6 A, top and bottom panel). FF50 was significantly reduced in both wild type and *Acta1*(D286G) diaphragm muscle strips (Fig. 6 A, top and bottom insets). The positive inotropic effect of *tirasemtiv* was not present at maximal stimulation frequencies (200 Hz) in wild type and *Acta1*(D286G) diaphragm muscle strips (Fig. 6 B, left and right panels). Acute *tirasemtiv* force values are shown in Table 4.

To assess the in vivo effect of *tirasemtiv* treatment on respiratory function, we performed whole-body plethysmography during acute and long-term *tirasemtiv* administration. Note that during these assays, *tirasemtiv* was present in the diaphragm muscles. Acute *tirasemtiv* treatment did not have any observable effects on RR, VT, or VE (Fig.6, C and D). Acute *tirasemtiv* plethysmography values are shown in Table 5. Thus, acute *tirasemtiv* exposure did not affect respiratory function in *Acta1*(D286G) mice.

Effect of long-term *tirasemtiv* treatment on respiratory function

Next, we assessed the effect of long-term *tirasemtiv* treatment on diaphragm muscle strips. We did not observe any changes in force production at any stimulation frequency nor differences in FF50 values (Fig. 7 A). Furthermore, no changes in tension were observed at maximal stimulation frequency in both groups (Fig. 7 B). Long-term *tirasemtiv* force values are shown in Table 6. Furthermore, long-term *tirasemtiv* treatment did not affect tidal volume and minute volume (Fig. 7, C and D, top and middle panels) but did significantly reduce the RR in *Acta1*(D286G)

Table 6. **In vitro diaphragm muscle mechanics—long-term *tirasemtiv* treatment**

Frequency (Hz)	1	5	10	20	40	60	80	100	150	# of mice	Age of mice in months
***Acta1*(Wt)—vehicle**										7	9
Absolute force (mN)	20 ± 8	22 ± 8	26 ± 10	41 ± 18	62 ± 24	71 ± 26	75 ± 26	76 ± 26	77 ± 26		
Normalized force (mN/mm^2)	40 ± 16	44 ± 16	51 ± 19	82 ± 38	122 ± 46	140 ± 46	147 ± 45	149 ± 45	150 ± 46		
Relative force (% of maximum)	27 ± 6	29 ± 7	34 ± 9	54 ± 16	80 ± 12	93 ± 8	98 ± 5	100 ± 3	100 ± 0.0		
***Acta1*(Wt)—*tirasemtiv*[a]**										8	9
Absolute force (mN)	24 ± 8	28 ± 11	34 ± 15	57 ± 20	81 ± 24	91 ± 25	95 ± 26	96 ± 26	97 ± 27		
Normalized force (mN/mm$^{2)}$	44 ± 16	51 ± 20	63 ± 26	105 ± 38	148 ± 44	165 ± 48	172 ± 44	174 ± 44	176 ± 44		
Relative force (% of maximum)	25 ± 6	29 ± 6	36 ± 13	58 ± 14	84 ± 9	93 ± 5	97 ± 3	99 ± 2	100 ± 0.0		
***Acta1*(D286G)—vehicle[b]**										15	9
Absolute force (mN)	21 ± 8	20 ± 8	22 ± 9	29 ± 15	47 ± 21	56 ± 23	60 ± 23	62 ± 23	64 ± 23		
Normalized force (mN/mm^2)	65 ± 26	59 ± 26	65 ± 28	84 ± 37	133 ± 49	159 ± 51	171 ± 50	177 ± 50	181 ± 51		
Relative force (% of maximum)	30 ± 9	33 ± 9	35 ± 9	45 ± 11	73 ± 14	87 ± 11	95 ± 5	98 ± 2	100 ± 0.0		
Acta1*(D286G)—*tirasemtiv										14	9
Absolute force (mN)	17 ± 7	20 ± 11	25 ± 16	33 ± 24	47 ± 27	54 ± 29	58 ± 30	60 ± 30	61 ± 31		
Normalized force (mN/mm^2)	51 ± 23	61 ± 19	75 ± 41	98 ± 70	140 ± 78	162 ± 82	174 ± 85	178 ± 86	183 ± 88		
Relative force (% of maximum)	29 ± 8	34 ± 9	41 ± 12	51 ± 19	76 ± 13	89 ± 10	95 ± 6	98 ± 3	100 ± 0.0		

[a]*Tirasemtiv* versus vehicle ($P < 0.05$).
[b]Acta1(D286G) versus Acta1(wt) ($P < 0.05$).

mice (Fig. 7 D, top panel). Long-term *Plethysmography* values are shown in Table 7. Thus, these data suggest that *tirasemtiv* improves ventilatory efficiency by maintaining VT and VE with fewer respiratory cycles.

Long-term effect of *tirasemtiv* on gene and protein expression and posttranslational modifications

We then assessed the effect of *tirasemtiv* on pathways involved in the regulation of muscle protein turnover. Muscle RING finger protein 1 (MuRF1) and atrogin-1 are muscle-specific E3 ligases that are involved in mediating muscle atrophy. We measured mRNA levels of both E3 ligases in GAS muscle after long-term *tirasemtiv* exposure. *Tirasemtiv* exposure significantly downregulated *MurRF-1* and *Atrogin-1* in wild type mice. In *Acta1*(D286G), *tirasemtiv* resulted in the upregulation of *atrogin-1* (Fig. 8 A), with no changes in *MuRF1* levels.

As dysfunctional mitochondria is a major source of reactive oxygen species, we aimed to assess whether *tirasemtiv* reduces the stress on such organelles. To this end, we assessed antioxidant levels in GAS muscle. No significant changes were observed in the protein levels of antioxidant enzymes superoxide dismutase 1 (SOD1) and Catalase (Fig. 8 B). Furthermore, we measured GAS total protein and MHC carbonylation. Such posttranslational modifications are implicated in skeletal muscle dysfunction in various chronic disorders (Barreiro et al., 2005a, 2005b; Li et al., 2015; Marin-Corral et al., 2009; Coirault et al., 2007). We observed that long-term *tirasemtiv* treatment had no effect on total protein carbonylation; however, it significantly reduced MHC carbonylation in both wild type and *Acta1*(D286G) mice (Fig. 8 C, bottom panel). Finally, we measured mitochondrial dynamic markers. Mitochondrial biogenesis, fission and fusion markers, such as peroxisome proliferator-activated receptor gamma coactivator 1-α (PGC-1α), Mitofusin-1 (MFN1), Mitofusin2 (MFN2), dynamin-like 120 kD protein (OPA1), dynamin-related protein 1 (DRP1), and mitochondrial fission 1 (FIS1) protein levels remain unchanged in both wild type and *Acta1*(D286G) mice after long-term *tirasemtiv* exposure (Fig. S1, A–C) for the exception of phosphorylated DRP1 (DRP1p616), which was significantly higher in *tirasemtiv*-treated wild type mice (Fig. 1 C, top panel).

Discussion

Here, we tested the ability of the fast skeletal muscle troponin activator *tirasemtiv* to improve muscle function in *Acta1*(D286G)

Table 7. **Plethysmography—long-term *tirasemtiv* treatment**

	Week 0[c]		Week 4[d]		# of mice	Age of mice in months
***Acta1*(Wt)—vehicle**					7	9
Respiratory rate (per minute)	315 ± 50	330 ± 17	255 ± 53	310 ± 24		
Tidal volume (ml/kg)	9.5 ± 2.2	14.6 ± 4	8.6 ± 1.2	13 ± 2.3		
Minute volume (ml/kg/minute)	3,027 ± 844	4,863 ± 1511	2,164 ± 480	4,040 ± 565		
***Acta1*(Wt)—*tirasemtiv*[a]**					8	9
Respiratory rate (per minute)	322 ± 44	331 ± 13	284 ± 50	310 ± 23		
Tidal volume (ml/kg)	8.9 ± 2	14.5 ± 3.2	7.9 ± 1.5	12.4 ± 1.7		
Minute volume (ml/kg/minute)	2,905 ± 698	4,782 ± 1,080	2,210 ± 450	3,848 ± 576		
***Acta1*(D286G)—vehicle[b]**					13	9
Respiratory rate (per minute)	357 ± 37	330 ± 23	319 ± 29	315 ± 25		
Tidal volume (ml/kg)	9.5 ± 2.1	14 ± 2.3	8.7 ± 1.7	14 ± 2.1		
Minute volume (ml/kg/minute)	3,396 ± 1,081	4,613 ± 812	2,724 ± 554	4,391 ± 768		
Acta1*(D286G)—*tirasemtiv					15	9
Respiratory rate (per minute)	331 ± 47	324 ± 19	270 ± 47	277[a] ± 37		
Tidal volume (ml/kg)	8.9 ± 1.4	14.5 ± 3	9.2 ± 2	14.3 ± 2.4		
Minute volume (ml/kg/minute)	2,924 ± 641	4,711 ± 1,012	2,392 ± 448	3,933 ± 827		

[a]*Tirasemtiv* versus vehicle ($P < 0.05$).
[b]Acta1(D286G) versus Acta1(wt) ($P < 0.05$).
[c]Week 2 versus Week 0 ($P < 0.05$).
[d]Week 4 versus Week 0 ($P < 0.05$).

mice. We show that acute and long-term *tirasemtiv* treatment significantly increases muscle contractile performance in vitro and in vivo at submaximal stimulation frequencies in both fast-twitch EDL and GAS and intermediate-twitch diaphragm muscles. The positive inotropic effect following acute and long-term *tirasemtiv* treatment is clinically relevant as most daily life activities, as well as tidal breathing, require submaximal muscle activation (Tikkanen et al., 2013; Jasmin and Gardiner, 1987). Altogether, our data support the potential positive therapeutic effect of fast skeletal muscle troponin activators in alleviating muscle weakness in a mouse model of NEM3.

Tirasemtiv improves skeletal muscle force-generating capacity and respiratory function in *Acta1*(D286G) mice

NEM is one of the most common forms of congenital myopathies, and, to date, no specific treatments are available. NEM causative genes encode proteins that are associated with the thin filament. Variants in thin filament genes such as *ACTA1* (NEM3) are usually associated with a severe congenital form often characterized by profound skeletal muscle weakness (antenatal or neonatal), myofibrillar disarrangement, and, in severe cases, death due to respiratory insufficiency (Labasse et al., 2022). However, milder forms of NEM3 have also been reported, with a mild disease progression (Agrawal et al., 2004; Witting et al., 2016; Feng and Marston, 2009; Laing et al., 2009). NEM3 caused by the p.Asp286Gly (D286G) variant is associated with a milder form of the disease. Previous work has shown that this variant reduces the calcium sensitivity of force in mouse myofibers (Ravenscroft et al., 2011a) and directly affects the binding of myosin cross-bridges to actin, thereby reducing the fraction of acto-myosin interactions in the strong binding state and contractile force (Ochala et al., 2012). Thus, increasing thin filament function may be an attractive approach to augment muscle function.

Our results are in line with our previous work performed on a more severe NEM3 mouse model with an *Acta1* p.His40Tyr variant (*Acta1*(H40Y)) (de Winter et al., 2021). Here, we show that acute *tirasemtiv* treatment results in a >50% increase in EDL muscle contractility in both wild type and *Acta1*(D286G) mice and a 45% and 64% increase in contractility in diaphragm muscle strips of *Acta1*(D286G) and wild type mice, respectively, at submaximal stimulation frequencies. Furthermore, we show that long-term *tirasemtiv* treatment via chow results in a significant increase in contractile force in EDL and GAS muscles at submaximal stimulations. This suggests that long-term administration of *tirasemtiv* does not desensitize fast twitch muscles. It should be noted, however, that we cannot rule out that the washout of *tirasemtiv* after long-term treatment was complete and did not confound our results.

In contrast to our previous work on an *Acta1*(H40Y) mouse model, here, we did not observe any significant improvements in EDL, GAS, or diaphragm muscle contractile function at maximal stimulation frequencies (de Winter et al., 2021). This may be explained by GAS and EDL muscles presenting with a more severe baseline phenotype in the *Acta1*(H40Y) model, with a significant reduction in maximal tension compared with the *Acta1*(D286G) model. Overall, acute and long-term *tirasemtiv* treatment had a significant positive inotropic effect on skeletal muscle contractile function at submaximal stimulation frequencies.

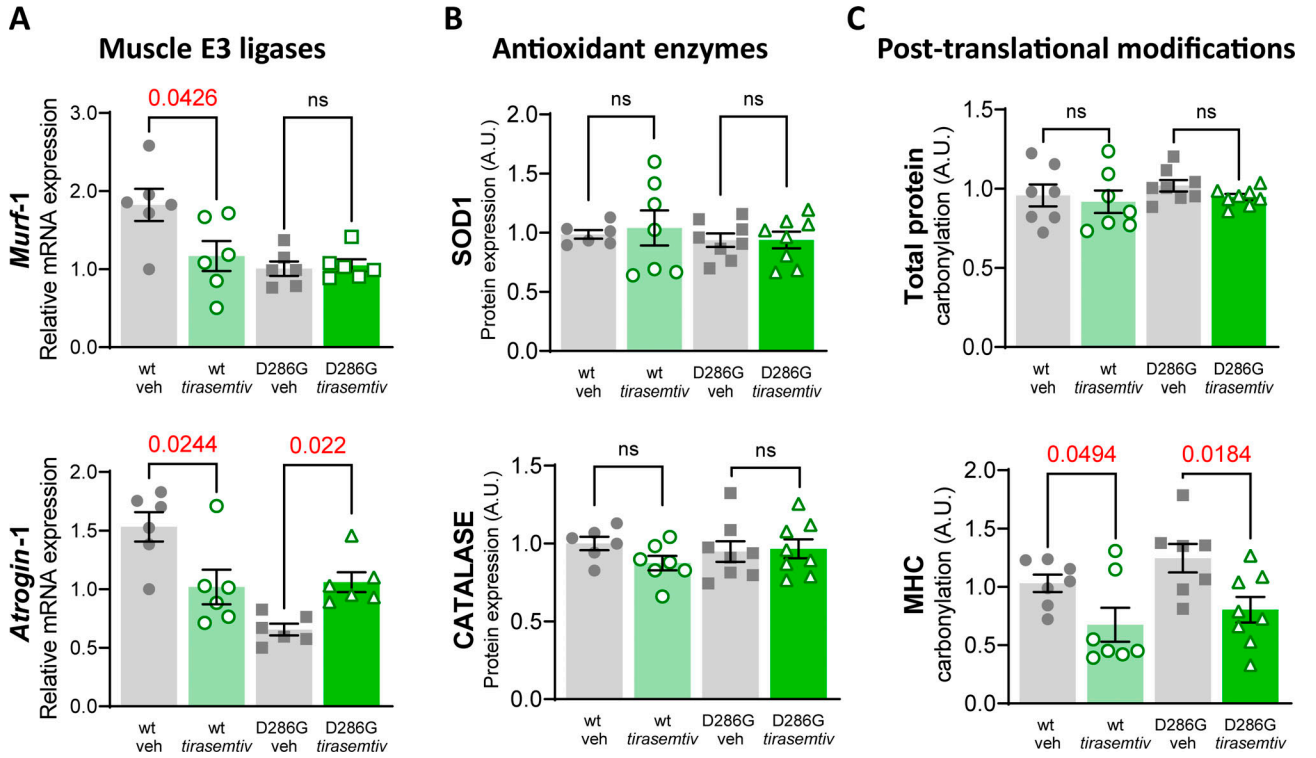

Figure 8. **Effect of long-term *tirasemtiv* administration on muscle mRNA and protein expression. (A)** Top panel and bottom panel: Relative mRNA levels of E3 ligases *Murf-1* and *Atrogin-1*, respectively, in wild type and *Acta*(D286G) *tirasemtiv* and vehicle treated GAS muscle. **(B)** Top panel and bottom panel: Total muscle protein and MHC carbonylation levels, respectively, in wild type and *Acta*(D286G) *tirasemtiv* and vehicle treated GAS muscle. **(C)** Top panel and bottom panel: Total muscle protein levels of antioxidant enzymes SOD1 and CATALASE, respectively, in wild type and *Acta*(D286G) *tirasemtiv* and vehicle treated GAS muscle.

In addition to peripheral skeletal muscle weakness, NEM patients also present with weakness of the respiratory muscles, i.e., intercostal muscles and the diaphragm (van Kleef et al., 2022), which can cause insufficient respiration and in severe cases respiratory failure and death. Our results show that acute *tirasemtiv* treatment has a strong positive inotropic effect on diaphragm contractility at submaximal stimulation frequencies. This effect is in line with previous work performed on other myopathic mouse models (Lee et al., 2019; Hwee et al., 2014). Additionally, at a clinical level, *tirasemtiv* has been shown to improve spirometric parameters in patients diagnosed with amyotrophic lateral sclerosis and myasthenia gravis (Shefner et al., 2013, 2019; Sanders et al., 2015). Unlike the results shown in previous work (Hwee et al., 2014; de Winter et al., 2021), here we did not see any improvements in VT, VE, or RR after acute *tirasemtiv* treatment. However, long-term *tirasemtiv* treatment in *Acta1*(D286G) mice showed a significant decrease in RR without affecting their VT or VE, suggesting perhaps a more efficient respiratory cycle.

Next to respiratory function, other important outcome parameters to assess treatment effects are the energy cost of contraction and resistance to fatigue. We have previously shown that *tirasemtiv* treatment significantly lowers the energy cost and improves resistance to fatigability in skeletal muscles in a more severe NEM3 mouse model (de Winter et al., 2021). This positive effect has also been observed in healthy rats treated with CK-2066260, a structural analog of *tirasemitiv*. CK-2066260 treatment significantly increased muscle endurance and resistance to fatigue without an increase in ATP demand or glycogen usage (Cheng et al., 2019). This effect might have potential benefits for NEM patients who present with insufficient respiration and in severe cases, respiratory failure. Future studies should address the effect of *tirasemtiv* on other respiratory muscles. In the present study we focused on the diaphragm; however, accessory respiratory muscles may benefit from fast skeletal muscle troponin activators as well. Previous work characterizing fiber type composition in human postmortem muscle tissue and patient's muscle biopsies showed that not only the diaphragm but also the accessory respiratory muscles (internal and external intercostal, scalene, and sternocleidomastoids muscles) and extra-thoracic muscles (rectus abdominis and transverse abdominis muscles) have a substantial percentage of fast-twitch muscle fibers on which *tirasemtiv* could potentially exert a positive ionotropic effect (Levine et al., 1997; Mizuno, 1991). Thus, *tirasemtiv* may result in a more efficient respiratory cycle and thereby alleviate respiratory muscle weakness in NEM patients.

Long-term *tirasemtiv* treatment reduces MHC carbonylation

A remarkable finding was the improved submaximal tension generation in EDL and GAS muscles of both wild type and *Acta1*(D286G) mice following long-term *tirasemtiv* treatment. Previous work on *Acta1*(D286G) mice has shown that the actomyosin interaction is altered (Ochala et al., 2012), which can in part explain the reduction in contractility. However, other changes in muscle, such as protein carbonylation, have been

associated with loss of muscle mass and muscle dysfunction in human chronic diseases and in animal models for different chronic conditions (Barreiro, 2016; Marin-Corral et al., 2010). Furthermore, altered redox balance may impair the acto–myosin interaction (Prochniewicz et al., 2008), and dysfunctional mitochondria can alter redox balance in mouse models of both moderate and mild forms of NEM3 (Tinklenberg et al., 2023), resulting in an increased oxidative stress and consequently, impaired muscle function, i.e., altered acto–myosin kinetics (Prochniewicz et al., 2008) and calcium sensitivity of force (Heunks et al., 2001). Interestingly, here, we show that *tirasemtiv* did not affect markers of mitochondrial biogenesis and antioxidant status. Furthermore, no changes in myofibrillar protein carbonylation following *tirasemtiv* treatment were found. We did however observe a significant reduction in MHC carbonylation in wild type and *Acta1*(D286G) mice after long-term *tirasemtiv* treatment. It appears that the effect of *tirasemtiv* on muscle contractility is independent of altered protein turnover and protein oxidation. Although speculative, the reduced MHC carbonylation may be a result of *tirasemtiv*'s effect on skeletal muscle energetics. *Tirasemtiv* reduces muscle energetic cost during activation (Cheng et al, 2019), which results in less free radicals, i.e., reactive oxygen and nitrogen species production. These radicals are known to impair muscle homeostasis and contractile function (Westerblad and Allen, 2011; Debold, 2015; Lian et al, 2022). Thus, we propose that *tirasemtiv* protects myofilament integrity by reducing free-radical production and consequently reducing MHC carbonylation. Future work should address the effect of *tirasemtiv* on other post-translational modifications such as ubiquitination, acetylation, citrullination, S-glutathiolation, and S-nitrosylation, which are known to also regulate muscle function and metabolism (Fert-Bober et al, 2015; Collins and Goldberg, 2017; Jeong et al, 2018; Kramer et al, 2018; Liang et al, 2022).

Clinical relevance

NEMs are among the most common forms of congenital myopathies. In the past years, our knowledge regarding the molecular mechanisms driving various subtypes of NEM has significantly advanced (Ravenscroft et al., 2018; Laitila and Wallgren-Pettersson, 2021, Sewry et al., 2019). However, there is still an unmet need for the development of specific therapies. Our data provide a proof-of-concept supporting the positive role of fast skeletal muscle troponin activators in improving muscle function during daily life activities that require submaximal activation. To date, fast skeletal muscle troponin activators have not been tested in clinical trials for NEM patients. We propose that fast skeletal muscle troponin activators may aid NEM patients by increasing muscle tension at submaximal stimulations and support coughing and respiratory muscle function during episodes of insufficient respiration. A phase III clinical trial showed poor tolerability of *tirasemtiv* in patients with amyotrophic lateral sclerosis (Shefner et al., 2019). However, in this phase III trial, authors did note that participants who tolerated the designated dose showed a trend toward increased respiratory function. The development of *tirasemtiv* analogs may further contribute to the development of specific treatments for NEM.

Data availability

The data are available from the corresponding author upon reasonable request.

Acknowledgments

Henk L. Granzier served as editor.

This study was supported by the ERA-NET E-Rare2 grant TREAT-NEMMYOP to C.A.C. Ottenheijm, J. Gondin, and R. Bottinelli; The Netherlands Organisation for Health Research and Development (ZonMW) VICI Grant 91819613 to C.A.C. Ottenheijm; and ZonMW-VENI Grant 09150161910168 to J.M. de Winter.

Author contributions: Conceptualization: C.A.C. Ottenheijm, J. Gondin, R. Bottinelli, and J.M. de Winter. Data curation: C.A.C. Ottenheijm, J.M. de Winter, R.A. Galli, T.C. Borsboom, J. Gondin, C. Gineste, R. Bottinelli, M.-A. Pellegrino, and M. Rossi. Formal analysis: R.A. Galli, T.C. Borsboom, C. Gineste, M. Rossi, and L. Brocca. Funding acquisition: C.A.C. Ottenheijm, R. Bottinelli, J. Gondin, and J.M. de Winter. Investigation: C.A.C. Ottenheijm, J.M. de Winter, T.C. Borsboom, C. Gineste, L. Brocca, M. Rossi, D.T. Hwee, F.I. Malik, R. Bottinelli, J. Gondin, and M.-A. Pellegrino. Methodology: C.A.C. Ottenheijm, J.M. de Winter, R. Bottinelli, M.-A. Pellegrino, and J. Gondin. Project administration: C.A.C. Ottenheijm and J.M. de Winter. Resources: C.A.C. Ottenheijm, J. Gondin, R. Bottinelli, J.M. de Winter, D.T. Hwee, and F.I. Malik. Supervision: C.A.C. Ottenheijm, J.M. de Winter, R. Bottinelli, J. Gondin, M.-A. Pellegrino, and L. Brocca. Visualization: R.A. Galli, C.A.C. Ottenheijm, and J.M. de Winter. Writing—original draft: R.A. Galli, C.A.C. Ottenheijm, and J.M. de Winter. Writing—review & editing: R.A. Galli, C.A.C. Ottenheijm, J.M. de Winter, J. Gondin, R. Bottinelli, C. Gineste, M.-A. Pellegrino, D.T. Hwee, and F.I. Malik.

Disclosures: D.T. Hwee reported other from Cytokinetics during the conduct of the study and other from Cytokinetics outside the submitted work. In addition, D.T. Hwee had a patent to *tirasemtiv* use issued for Cytokinetics. F.I. Malik reported personal fees from Cytokinetics, Inc. during the conduct of the study and personal fees from Cytokinetics, Inc. outside the submitted work. F.I. Malik also had a patent to *tirasemtiv* patent licensed to Cytokinetics. No other disclosures were reported.

Submitted: 22 August 2023
Revised: 1 December 2023
Accepted: 30 January 2024

References

Agrawal, P.B., R.S. Greenleaf, K.K. Tomczak, V.L. Lehtokari, C. Wallgren-Pettersson, W. Wallefeld, N.G. Laing, B.T. Darras, S.K. Maciver, P.R. Dormitzer, and A.H. Beggs. 2007. Nemaline myopathy with minicores caused by mutation of the CFL2 gene encoding the skeletal muscle actin-binding protein, cofilin-2. *Am. J. Hum. Genet.* 80:162–167. https://doi.org/10.1086/510402

Agrawal, P.B., C.D. Strickland, C. Midgett, A. Morales, D.E. Newburger, M.A. Poulos, K.K. Tomczak, M.M. Ryan, S.T. Iannaccone, T.O. Crawford, et al. 2004. Heterogeneity of nemaline myopathy cases with skeletal muscle alpha-actin gene mutations. *Ann. Neurol.* 56:86–96. https://doi.org/10.1002/ana.20157

Andrews, J.A., T.M. Miller, V. Vijayakumar, R. Stoltz, J.K. James, L. Meng, A.A. Wolff, and F.I. Malik. 2018. CK-2127107 amplifies skeletal muscle response to nerve activation in humans. *Muscle Nerve*. 57:729–734. https://doi.org/10.1002/mus.26017

Barreiro, E. 2016. Role of protein carbonylation in skeletal muscle mass loss associated with chronic conditions. *Proteomes*. 4:18. https://doi.org/10.3390/proteomes4020018

Barreiro, E., B. de la Puente, J. Minguella, J.M. Corominas, S. Serrano, S.N. Hussain, and J. Gea. 2005a. Oxidative stress and respiratory muscle dysfunction in severe chronic obstructive pulmonary disease. *Am. J. Respir. Crit. Care Med.* 171:1116–1124. https://doi.org/10.1164/rccm.200407-887OC

Barreiro, E., J. Gea, M. Di Falco, L. Kriazhev, S. James, and S.N. Hussain. 2005b. Protein carbonyl formation in the diaphragm. *Am. J. Respir. Cell Mol. Biol.* 32:9–17. https://doi.org/10.1165/rcmb.2004-0021OC

Cannavino, J., L. Brocca, M. Sandri, B. Grassi, R. Bottinelli, and M.A. Pellegrino. 2015. The role of alterations in mitochondrial dynamics and PGC-1α overexpression in fast muscle atrophy following hindlimb unloading. *J. Physiol.* 593:1981–1995. https://doi.org/10.1113/jphysiol.2014.286740

Cheng, A.J., D.T. Hwee, L.H. Kim, N. Durham, H.T. Yang, A.C. Hinken, A.R. Kennedy, R.L. Terjung, J.R. Jasper, F.I. Malik, and H. Westerblad. 2019. Fast skeletal muscle troponin activator CK-2066260 increases fatigue resistance by reducing the energetic cost of muscle contraction. *J. Physiol.* 597:4615–4625. https://doi.org/10.1113/JP278235

Coirault, C., A. Guellich, T. Barbry, J.L. Samuel, B. Riou, and Y. Lecarpentier. 2007. Oxidative stress of myosin contributes to skeletal muscle dysfunction in rats with chronic heart failure. *Am. J. Physiol. Heart Circ. Physiol.* 292:H1009–H1017. https://doi.org/10.1152/ajpheart.00438.2006

Collins, G.A., and A.L. Goldberg. 2017. The logic of the 26S proteasome. *Cell*. 169:792–806. https://doi.org/10.1016/j.cell.2017.04.023

Colombo, I., M. Scoto, A.Y. Manzur, S.A. Robb, L. Maggi, V. Gowda, T. Cullup, M. Yau, R. Phadke, C. Sewry, et al. 2015. Congenital myopathies: Natural history of a large pediatric cohort. *Neurology*. 84:28–35. https://doi.org/10.1212/WNL.0000000000001110

de Winter, J.M., D. Buck, C. Hidalgo, J.R. Jasper, F.I. Malik, N.F. Clarke, G.J. Stienen, M.W. Lawlor, A.H. Beggs, C.A. Ottenheijm, and H. Granzier. 2013. Troponin activator augments muscle force in nemaline myopathy patients with nebulin mutations. *J. Med. Genet.* 50:383–392. https://doi.org/10.1136/jmedgenet-2012-101470

de Winter, J.M., C. Gineste, E. Minardi, L. Brocca, M. Rossi, T. Borsboom, A.H. Beggs, M. Bernard, D. Bendahan, D.T. Hwee, et al. 2021. Acute and chronic tirasemtiv treatment improves in vivo and in vitro muscle performance in actin-based nemaline myopathy mice. *Hum. Mol. Genet.* 30:1305–1320. https://doi.org/10.1093/hmg/ddab112

de Winter, J.M., J.P. Molenaar, M. Yuen, R. van der Pijl, S. Shen, S. Conijn, M. van de Locht, M. Willigenburg, S.J. Bogaards, E.S. van Kleef, et al. 2020. KBTBD13 is an actin-binding protein that modulates muscle kinetics. *J. Clin. Invest.* 130:754–767. https://doi.org/10.1172/JCI124000

de Winter, J.M., and C.A.C. Ottenheijm. 2017. Sarcomere dysfunction in nemaline myopathy. *J. Neuromuscul. Dis.* 4:99–113. https://doi.org/10.3233/JND-160200

Debold, E.P. 2015. Potential molecular mechanisms underlying muscle fatigue mediated by reactive oxygen and nitrogen species. *Front. Physiol.* 6:239. https://doi.org/10.3389/fphys.2015.00239

Donner, K., M. Ollikainen, M. Ridanpää, H.J. Christen, H.H. Goebel, M. de Visser, K. Pelin, and C. Wallgren-Pettersson. 2002. Mutations in the beta-tropomyosin (TPM2) gene--a rare cause of nemaline myopathy. *Neuromuscul. Disord.* 12:151–158. https://doi.org/10.1016/S0960-8966(01)00252-8

Feng, J.J., and S. Marston. 2009. Genotype-phenotype correlations in ACTA1 mutations that cause congenital myopathies. *Neuromuscul. Disord.* 19:6–16. https://doi.org/10.1016/j.nmd.2008.09.005

Fert-Bober, J., J.T. Giles, R.J. Holewinski, J.A. Kirk, H. Uhrigshardt, E.L. Crowgey, F. Andrade, C.O. Bingham III, J.K. Park, M.K. Halushka, et al. 2015. Citrullination of myofilament proteins in heart failure. *Cardiovasc. Res.* 108:232–242. https://doi.org/10.1093/cvr/cvv185

Giannesini, B., C. Vilmen, Y. Le Fur, C. Dalmasso, P.J. Cozzone, and D. Bendahan. 2010. A strictly noninvasive MR setup dedicated to longitudinal studies of mechanical performance, bioenergetics, anatomy, and muscle recruitment in contracting mouse skeletal muscle. *Magn. Reson. Med.* 64:262–270. https://doi.org/10.1002/mrm.22386

Gineste, C., J.M. De Winter, C. Kohl, C.C. Witt, B. Giannesini, K. Brohm, Y. Le Fur, N. Gretz, C. Vilmen, E. Pecchi, et al. 2013a. In vivo and in vitro investigations of heterozygous nebulin knock-out mice disclose a mild skeletal muscle phenotype. *Neuromuscul. Disord.* 23:357–369. https://doi.org/10.1016/j.nmd.2012.12.011

Gineste, C., G. Duhamel, Y. Le Fur, C. Vilmen, P.J. Cozzone, K.J. Nowak, D. Bendahan, and J. Gondin. 2013b. Multimodal MRI and (31)P-MRS investigations of the ACTA1(Asp286Gly) mouse model of nemaline myopathy provide evidence of impaired in vivo muscle function, altered muscle structure and disturbed energy metabolism. *PLoS One*. 8:e72294. https://doi.org/10.1371/journal.pone.0072294

Gupta, V.A., G. Ravenscroft, R. Shaheen, E.J. Todd, L.C. Swanson, M. Shiina, K. Ogata, C. Hsu, N.F. Clarke, B.T. Darras, et al. 2013. Identification of KLHL41 mutations implicates BTB-Kelch-mediated ubiquitination as an alternate pathway to myofibrillar disruption in nemaline myopathy. *Am. J. Hum. Genet.* 93:1108–1117. https://doi.org/10.1016/j.ajhg.2013.10.020

Hansen, R., K.G. Saikali, W. Chou, A.J. Russell, M.M. Chen, V. Vijayakumar, R.R. Stoltz, S. Baudry, R.M. Enoka, D.J. Morgans, et al. 2014. Tirasemtiv amplifies skeletal muscle response to nerve activation in humans. *Muscle Nerve*. 50:925–931. https://doi.org/10.1002/mus.24239

Heunks, L.M., M.J. Cody, P.C. Geiger, P.N. Dekhuijzen, and G.C. Sieck. 2001. Nitric oxide impairs Ca^{2+} activation and slows cross-bridge cycling kinetics in skeletal muscle. *J. Appl. Physiol.* 91:2233–2239. https://doi.org/10.1152/jappl.2001.91.5.2233

Hwee, D.T., A. Kennedy, J. Ryans, A.J. Russell, Z. Jia, A.C. Hinken, D.J. Morgans, F.I. Malik, and J.R. Jasper. 2014. Fast skeletal muscle troponin activator tirasemtiv increases muscle function and performance in the B6SJL-SOD1G93A ALS mouse model. *PLoS One*. 9:e96921. https://doi.org/10.1371/journal.pone.0096921

Ilkovski, B., S.T. Cooper, K. Nowak, M.M. Ryan, N. Yang, C. Schnell, H.J. Durling, L.G. Roddick, I. Wilkinson, A.J. Kornberg, et al. 2001. Nemaline myopathy caused by mutations in the muscle alpha-skeletal-actin gene. *Am. J. Hum. Genet.* 68:1333–1343. https://doi.org/10.1086/320605

Jasmin, B.J., and P.F. Gardiner. 1987. Patterns of EMG activity of rat plantaris muscle during swimming and other locomotor activities. *J. Appl. Physiol.* 63:713–718. https://doi.org/10.1152/jappl.1987.63.2.713

Jeong, E.M., C.Z. Jin, J.H. Jang, Z.H. Zhao, C.L. Jin, J.H. Lee, K.B. Lee, S.J. Kim, I.G. Kim, and Y.H. Zhang. 2018. S-nitrosylation of transglutaminase 2 impairs fatty acid-stimulated contraction in hypertensive cardiomyocytes. *Exp. Mol. Med.* 50:1–11. https://doi.org/10.1038/s12276-017-0021-x

Johnston, J.J., R.I. Kelley, T.O. Crawford, D.H. Morton, R. Agarwala, T. Koch, A.A. Schäffer, C.A. Francomano, and L.G. Biesecker. 2000. A novel nemaline myopathy in the Amish caused by a mutation in troponin T1. *Am. J. Hum. Genet.* 67:814–821. https://doi.org/10.1086/303089

Joureau, B., J.M. de Winter, S. Conijn, S.J.P. Bogaards, I. Kovacevic, A. Kalganov, M. Persson, J. Lindqvist, G.J.M. Stienen, T.C. Irving, et al. 2018. Dysfunctional sarcomere contractility contributes to muscle weakness in ACTA1-related nemaline myopathy (NEM3). *Ann. Neurol.* 83:269–282. https://doi.org/10.1002/ana.25144

Kramer, P.A., J. Duan, M.J. Gaffrey, A.K. Shukla, L. Wang, T.K. Bammler, W.J. Qian, and D.J. Marcinek. 2018. Fatiguing contractions increase protein S-glutathionylation occupancy in mouse skeletal muscle. *Redox Biol.* 17:367–376. https://doi.org/10.1016/j.redox.2018.05.011

Labasse, C., G. Brochier, A.L. Taratuto, B. Cadot, J. Rendu, S. Monges, V. Biancalana, S. Quijano-Roy, M.T. Bui, A. Chanut, et al. 2022. Severe ACTA1-related nemaline myopathy: Intranuclear rods, cytoplasmic bodies, and enlarged perinuclear space as characteristic pathological features on muscle biopsies. *Acta Neuropathol. Commun.* 10:101. https://doi.org/10.1186/s40478-022-01400-0

Laemmli, U.K. 1970. Cleavage of structural proteins during the assembly of the head of bacteriophage T4. *Nature*. 227:680–685. https://doi.org/10.1038/227680a0

Laing, N.G., D.E. Dye, C. Wallgren-Pettersson, G. Richard, N. Monnier, S. Lillis, T.L. Winder, H. Lochmüller, C. Graziano, S. Mitrani-Rosenbaum, et al. 2009. Mutations and polymorphisms of the skeletal muscle alpha-actin gene (ACTA1). *Hum. Mutat.* 30:1267–1277. https://doi.org/10.1002/humu.21059

Laing, N.G., S.D. Wilton, P.A. Akkari, S. Dorosz, K. Boundy, C. Kneebone, P. Blumbergs, S. White, H. Watkins, D.R. Love, and E. Haan. 1995. A mutation in the alpha tropomyosin gene TPM3 associated with autosomal dominant nemaline myopathy. *Nat. Genet.* 9:75–79. https://doi.org/10.1038/ng0195-75

Laitila, J., and C. Wallgren-Pettersson. 2021. Recent advances in nemaline myopathy. *Neuromuscul. Disord.* 31:955–967. https://doi.org/10.1016/j.nmd.2021.07.012

Lee, E.J., J. Kolb, D.T. Hwee, F.I. Malik, and H.L. Granzier. 2019. Functional characterization of the intact diaphragm in a nebulin-based nemaline myopathy (NM) model-effects of the fast skeletal muscle troponin

activator tirasemtiv. *Int. J. Mol. Sci.* 20:5008. https://doi.org/10.3390/ijms20205008

Levine, S., L. Kaiser, J. Leferovich, and B. Tikunov. 1997. Cellular adaptations in the diaphragm in chronic obstructive pulmonary disease. *N. Engl. J. Med.* 337:1799–1806. https://doi.org/10.1056/NEJM199712183372503

Li, M., H. Ogilvie, J. Ochala, K. Artemenko, H. Iwamoto, N. Yagi, J. Bergquist, and L. Larsson. 2015. Aberrant post-translational modifications compromise human myosin motor function in old age. *Aging Cell.* 14: 228–235. https://doi.org/10.1111/acel.12307

Li, M.X., P. Mercier, J.J. Hartman, and B.D. Sykes. 2021. Structural basis of Tirasemtiv activation of fast skeletal muscle. *J. Med. Chem.* 64: 3026–3034. https://doi.org/10.1021/acs.jmedchem.0c01412

Lian, D., M.M. Chen, H. Wu, S. Deng, and X. Hu. 2022. The role of oxidative stress in skeletal muscle myogenesis and muscle disease. *Antioxidants*. 11:755. https://doi.org/10.3390/antiox11040755

Liang, D., C. Chen, S. Huang, S. Liu, L. Fu, and Y. Niu. 2022. Alterations of lysine acetylation profile in murine skeletal muscles upon exercise. *Front. Aging Neurosci.* 14:859313. https://doi.org/10.3389/fnagi.2022.859313

Lindqvist, J., A.J. Cheng, G. Renaud, E.C. Hardeman, and J. Ochala. 2013. Distinct underlying mechanisms of limb and respiratory muscle fiber weaknesses in nemaline myopathy. *J. Neuropathol. Exp. Neurol.* 72: 472–481. https://doi.org/10.1097/NEN.0b013e318293b1cc

Malfatti, E., J. Böhm, E. Lacène, M. Beuvin, N.B. Romero, and J. Laporte. 2015. A premature stop codon in MYO18B is associated with severe nemaline myopathy with cardiomyopathy. *J. Neuromuscul. Dis.* 2:219–227. https://doi.org/10.3233/JND-150085

Marin-Corral, J., C.C. Fontes, S. Pascual-Guardia, F. Sanchez, M. Olivan, J.M. Argilés, S. Busquets, F.J. López-Soriano, and E. Barreiro. 2010. Redox balance and carbonylated proteins in limb and heart muscles of cachectic rats. *Antioxid. Redox Signal.* 12:365–380. https://doi.org/10.1089/ars.2009.2818

Marin-Corral, J., J. Minguella, A.L. Ramírez-Sarmiento, S.N. Hussain, J. Gea, and E. Barreiro. 2009. Oxidised proteins and superoxide anion production in the diaphragm of severe COPD patients. *Eur. Respir. J.* 33: 1309–1319. https://doi.org/10.1183/09031936.00072008

Marston, S., M. Mirza, H. Abdulrazzak, and C. Sewry. 2004. Functional characterisation of a mutant actin (Met132Val) from a patient with nemaline myopathy. *Neuromuscul. Disord.* 14:167–174. https://doi.org/10.1016/j.nmd.2003.11.003

Miyatake, S., S. Mitsuhashi, Y.K. Hayashi, E. Purevjav, A. Nishikawa, E. Koshimizu, M. Suzuki, K. Yatabe, Y. Tanaka, K. Ogata, et al. 2017. Biallelic mutations in MYPN, encoding myopalladin, are associated with childhood-onset, slowly progressive nemaline myopathy. *Am. J. Hum. Genet.* 100:169–178. https://doi.org/10.1016/j.ajhg.2016.11.017

Mizuno, M. 1991. Human respiratory muscles: Fibre morphology and capillary supply. *Eur. Respir. J.* 4:587–601. https://doi.org/10.1183/09031936.93.04050587

Nguyen, M.A., J.E. Joya, A.J. Kee, A. Domazetovska, N. Yang, J.W. Hook, F.A. Lemckert, E. Kettle, V.A. Valova, P.J. Robinson, et al. 2011. Hypertrophy and dietary tyrosine ameliorate the phenotypes of a mouse model of severe nemaline myopathy. *Brain.* 134:3516–3529. https://doi.org/10.1093/brain/awr274

Ochala, J. 2008. Thin filament proteins mutations associated with skeletal myopathies: Defective regulation of muscle contraction. *J. Mol. Med.* 86: 1197–1204. https://doi.org/10.1007/s00109-008-0380-9

Ochala, J., H. Iwamoto, L. Larsson, and N. Yagi. 2010. A myopathy-linked tropomyosin mutation severely alters thin filament conformational changes during activation. *Proc. Natl. Acad. Sci. USA.* 107:9807–9812. https://doi.org/10.1073/pnas.1001733107

Ochala, J., G. Ravenscroft, N.G. Laing, and K.J. Nowak. 2012. Nemaline myopathy-related skeletal muscle α-actin (ACTA1) mutation, Asp286Gly, prevents proper strong myosin binding and triggers muscle weakness. *PLoS One.* 7:e45923. https://doi.org/10.1371/journal.pone.0045923

Ochala, J., G. Ravenscroft, E. McNamara, K.J. Nowak, and H. Iwamoto. 2015. X-ray recordings reveal how a human disease-linked skeletal muscle α-actin mutation leads to contractile dysfunction. *J. Struct. Biol.* 192: 331–335. https://doi.org/10.1016/j.jsb.2015.09.008

Ottenheijm, C.A., P. Hooijman, E.T. DeChene, G.J. Stienen, A.H. Beggs, and H. Granzier. 2010. Altered myofilament function depresses force generation in patients with nebulin-based nemaline myopathy (NEM2). *J. Struct. Biol.* 170:334–343. https://doi.org/10.1016/j.jsb.2009.11.013

Pelin, K., P. Hilpelä, K. Donner, C. Sewry, P.A. Akkari, S.D. Wilton, D. Wattanasirichaigoon, M.L. Bang, T. Centner, F. Hanefeld, et al. 1999. Mutations in the nebulin gene associated with autosomal recessive nemaline myopathy. *Proc. Natl. Acad. Sci. USA.* 96:2305–2310. https://doi.org/10.1073/pnas.96.5.2305

Pellegrino, M.A., M. Canepari, R. Rossi, G. D'Antona, C. Reggiani, and R. Bottinelli. 2003. Orthologous myosin isoforms and scaling of shortening velocity with body size in mouse, rat, rabbit and human muscles. *J. Physiol.* 546:677–689. https://doi.org/10.1113/jphysiol.2002.027375

Prochniewicz, E., D.A. Lowe, D.J. Spakowicz, L. Higgins, K. O'Conor, L.V. Thompson, D.A. Ferrington, and D.D. Thomas. 2008. Functional, structural, and chemical changes in myosin associated with hydrogen peroxide treatment of skeletal muscle fibers. *Am. J. Physiol. Cell Physiol.* 294:C613–C626. https://doi.org/10.1152/ajpcell.00232.2007

Ravenscroft, G., R.J. Bryson-Richardson, K.J. Nowak, and N.G. Laing. 2018. Recent advances in understanding congenital myopathies. *F1000 Res.* 7: F1000 Faculty Rev-1921. https://doi.org/10.12688/f1000research.16422.1

Ravenscroft, G., C. Jackaman, S. Bringans, J.M. Papadimitriou, L.M. Griffiths, E. McNamara, A.J. Bakker, K.E. Davies, N.G. Laing, and K.J. Nowak. 2011a. Mouse models of dominant ACTA1 disease recapitulate human disease and provide insight into therapies. *Brain.* 134:1101–1115. https://doi.org/10.1093/brain/awr004

Ravenscroft, G., C. Jackaman, C.A. Sewry, E. McNamara, S.E. Squire, A.C. Potter, J. Papadimitriou, L.M. Griffiths, A.J. Bakker, K.E. Davies, et al. 2011b. Actin nemaline myopathy mouse reproduces disease, suggests other actin disease phenotypes and provides cautionary note on muscle transgene expression. *PLoS One.* 6:e28699. https://doi.org/10.1371/journal.pone.0028699

Ravenscroft, G., S. Miyatake, V.L. Lehtokari, E.J. Todd, P. Vornanen, K.S. Yau, Y.K. Hayashi, N. Miyake, Y. Tsurusaki, H. Doi, et al. 2013. Mutations in KLHL40 are a frequent cause of severe autosomal-recessive nemaline myopathy. *Am. J. Hum. Genet.* 93:6–18. https://doi.org/10.1016/j.ajhg.2013.05.004

Russell, A.J., J.J. Hartman, A.C. Hinken, A.R. Muci, R. Kawas, L. Driscoll, G. Godinez, K.H. Lee, D. Marquez, W.F.T. Browne IV, et al. 2012. Activation of fast skeletal muscle troponin as a potential therapeutic approach for treating neuromuscular diseases. *Nat. Med.* 18:452–455. https://doi.org/10.1038/nm.2618

Ryan, M.M., C. Schnell, C.D. Strickland, L.K. Shield, G. Morgan, S.T. Iannaccone, N.G. Laing, A.H. Beggs, and K.N. North. 2001. Nemaline myopathy: A clinical study of 143 cases. *Ann. Neurol.* 50:312–320. https://doi.org/10.1002/ana.1080

Sambuughin, N., K.S. Yau, M. Olivé, R.M. Duff, M. Bayarsaikhan, S. Lu, L. Gonzalez-Mera, P. Sivadorai, K.J. Nowak, G. Ravenscroft, et al. 2010. Dominant mutations in KBTBD13, a member of the BTB/Kelch family, cause nemaline myopathy with cores. *Am. J. Hum. Genet.* 87:842–847. https://doi.org/10.1016/j.ajhg.2010.10.020

Sandaradura, S.A., A. Bournazos, A. Mallawaarachchi, B.B. Cummings, L.B. Waddell, K.J. Jones, C. Troedson, A. Sudarsanam, B.M. Nash, G.B. Peters, et al. 2018. Nemaline myopathy and distal arthrogryposis associated with an autosomal recessive TNNT3 splice variant. *Hum. Mutat.* 39: 383–388. https://doi.org/10.1002/humu.23385

Sanders, D.B., J. Rosenfeld, M.M. Dimachkie, L. Meng, F.I. Malik, and Tirasemtiv in Myasthenia Gravis Study Group. 2015. A double-blinded, randomized, placebo-controlled trial to evaluate efficacy, safety, and tolerability of single doses of tirasemtiv in patients with acetylcholine receptor-binding antibody-positive myasthenia gravis. *Neurotherapeutics.* 12:455–460. https://doi.org/10.1007/s13311-015-0345-y

Sanoudou, D., and A.H. Beggs. 2001. Clinical and genetic heterogeneity in nemaline myopathy: A disease of skeletal muscle thin filaments. *Trends Mol. Med.* 7:362–368. https://doi.org/10.1016/S1471-4914(01)02089-5

Schneider, C.A., W.S. Rasband, and K.W. Eliceiri. 2012. NIH image to ImageJ: 25 years of image analysis. *Nat. Methods.* 9:671–675. https://doi.org/10.1038/nmeth.2089

Sewry, C.A., J.M. Laitila, and C. Wallgren-Pettersson. 2019. Nemaline myopathies: A current view. *J. Muscle Res. Cell Motil.* 40:111–126. https://doi.org/10.1007/s10974-019-09519-9

Shefner, J.M., M.E. Cudkowicz, O. Hardiman, B.M. Cockcroft, J.H. Lee, F.I. Malik, L. Meng, S.A. Rudnicki, A.A. Wolff, J.A. Andrews, and VITALITY-ALS Study Group. 2019. A phase III trial of tirasemtiv as a potential treatment for amyotrophic lateral sclerosis. *Amyotroph. Lateral Scler. Frontotemporal Degener.* 0:1–11. https://doi.org/10.1080/21678421.2019.1612922

Shefner, J.M., M.L. Watson, L. Meng, A.A. Wolff, and Neals/Cytokinetics STUDY Team. 2013. A study to evaluate safety and tolerability of repeated doses of tirasemtiv in patients with amyotrophic lateral

sclerosis. *Amyotroph. Lateral Scler. Frontotemporal Degener.* 14:574–581. https://doi.org/10.3109/21678421.2013.822517

Tikkanen, O., P. Haakana, A.J. Pesola, K. Häkkinen, T. Rantalainen, M. Havu, T. Pullinen, and T. Finni. 2013. Muscle activity and inactivity periods during normal daily life. *PLoS One.* 8:e52228. https://doi.org/10.1371/journal.pone.0052228

Tinklenberg, J.A., R.A. Slick, J. Sutton, L. Zhang, H. Meng, M.J. Beatka, M. Vanden Avond, M.J. Prom, E. Ott, F. Montanaro, et al. 2023. Different mouse models of nemaline myopathy harboring Acta1 mutations display differing abnormalities related to mitochondrial biology. *Am. J. Pathol.* 193:1548–1567. https://doi.org/10.1016/j.ajpath.2023.06.008

van de Locht, M., T.C. Borsboom, J.M. Winter, and C.A.C. Ottenheijm. 2021. Troponin variants in congenital myopathies: How they affect skeletal muscle mechanics. *Int. J. Mol. Sci.* 22:9187. https://doi.org/10.3390/ijms22179187

van Kleef, E.S.B., J.L.M. van Doorn, M.A. Gaytant, W. de Weerd, B.A.H. Vosse, C. Wallgren-Pettersson, B.G.M. van Engelen, C.A.C. Ottenheijm, N.C. Voermans, and J. Doorduin. 2022. Respiratory muscle function in patients with nemaline myopathy. *Neuromuscul. Disord.* 32:654–663. https://doi.org/10.1016/j.nmd.2022.06.009

Vandamme, D., E. Lambert, D. Waterschoot, C. Cognard, J. Vandekerckhove, C. Ampe, B. Constantin, and H. Rommelaere. 2009. Alpha-Skeletal muscle actin nemaline myopathy mutants cause cell death in cultured muscle cells. *Biochim. Biophys. Acta.* 1793:1259–1271. https://doi.org/10.1016/j.bbamcr.2009.04.004

Wallgren-Pettersson, C., C.A. Sewry, K.J. Nowak, and N.G. Laing. 2011. Nemaline myopathies. *Semin. Pediatr. Neurol.* 18:230–238. https://doi.org/10.1016/j.spen.2011.10.004

Westerblad, H., and D.G. Allen. 2011. Emerging roles of ROS/RNS in muscle function and fatigue. *Antioxid. Redox Signal.* 15:2487–2499. https://doi.org/10.1089/ars.2011.3909

Winter, J.M., B. Joureau, E.J. Lee, B. Kiss, M. Yuen, V.A. Gupta, C.T. Pappas, C.C. Gregorio, G.J. Stienen, S. Edvardson, et al. 2016. Mutation-specific effects on thin filament length in thin filament myopathy. *Ann. Neurol.* 79:959–969. https://doi.org/10.1002/ana.24654

Witting, N., U. Werlauff, M. Duno, and J. Vissing. 2016. Prevalence and phenotypes of congenital myopathy due to α-actin 1 gene mutations. *Muscle Nerve.* 53:388–393. https://doi.org/10.1002/mus.24765

Yin, X., C.Q. Pu, Q. Wang, J.X. Liu, and Y.L. Mao. 2014. Clinical and pathological features of patients with nemaline myopathy. *Mol. Med. Rep.* 10:175–182. https://doi.org/10.3892/mmr.2014.2184

Yuen, M., S.A. Sandaradura, J.J. Dowling, A.S. Kostyukova, N. Moroz, K.G. Quinlan, V.L. Lehtokari, G. Ravenscroft, E.J. Todd, O. Ceyhan-Birsoy, et al. 2015. Leiomodin-3 dysfunction results in thin filament disorganization and nemaline myopathy. *J. Clin. Invest.* 125:456–457. https://doi.org/10.1172/JCI80057

Supplemental material

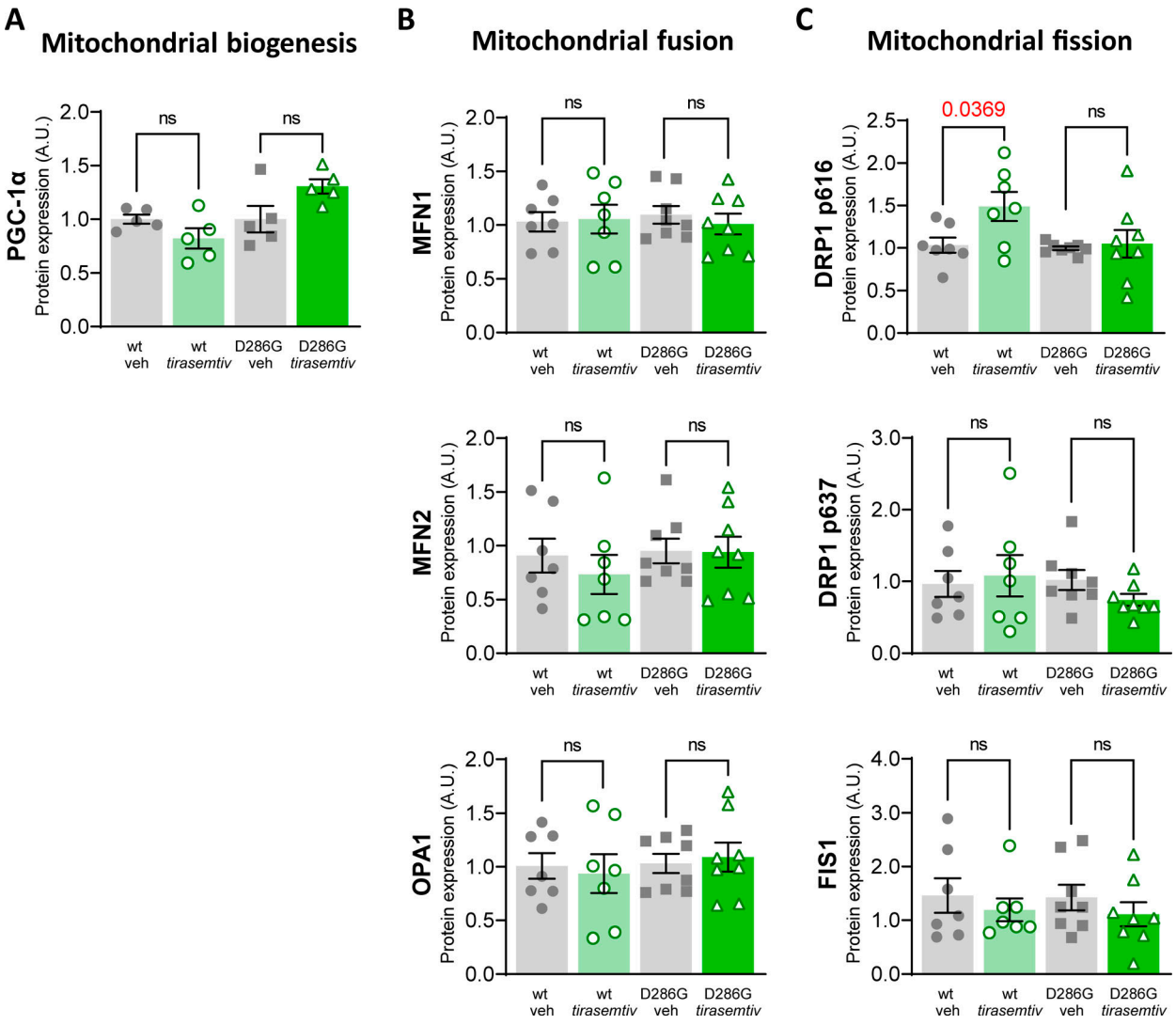

Figure S1. **Effect of long-term *tirasemtiv* administration protein expression of muscle mitochondrial dynamic markers.** All mitochondrial markers were measured in GAS muscles. **(A)** Protein levels of mitochondrial biogenesis marker PGC-1α in GAS muscles of wild type and *Acta*(D286G) vehicle and *tirasemtiv*-treated mice. **(B)** Top, middle, and bottom panels: Protein levels of mitochondrial fusion markers MFN1, MNF2, and OPA1, respectively, in GAS muscles of wild type and *Acta*(D286G) vehicle and *tirasemtiv*-treated mice. **(C)** Top, middle, and bottom panels: Protein levels of mitochondrial fission markers DRP1 p616, DRP1 p637, and FIS1, respectively, in GAS muscles of wild type and *Acta*(D286G) vehicle and *tirasemtiv*-treated mice.